Published for SISSA by Springer

Received: October 3, 2017
Revised: December 28, 2017
Accepted: January 23, 2018
Published: February 1, 2018

Higgs production at future e^+e^- colliders in the Georgi-Machacek model

Bin Li,[a,1] **Zhi-Long Han**[b] **and Yi Liao**[a,c,d]

[a] *School of Physics, Nankai University, Tianjin 300071, China*
[b] *School of Physics and Technology, University of Jinan, Jinan, Shandong 250022, China*
[c] *CAS Key Laboratory of Theoretical Physics, Institute of Theoretical Physics, Chinese Academy of Sciences, Beijing 100190, China*
[d] *Center for High Energy Physics, Peking University, Beijing 100871, China*

E-mail: libin@pku.edu.cn, sps_hanzl@ujn.edu.cn, liaoy@nankai.edu.cn

Abstract: We study how the dominant single and double SM-like Higgs (h) production at future e^+e^- colliders is modified in the Georgi-Machacek (GM) model. On imposing theoretical, indirect and direct constraints, significant deviations of h-couplings from their SM values are still possible; for instance, the Higgs-gauge coupling can be corrected by a factor $\kappa_{hVV} \in [0.93, 1.15]$ in the allowed parameter space. For the Higgs-strahlung $e^+e^- \to hZ$ and vector boson fusion processes $e^+e^- \to h\nu\bar{\nu}$, he^+e^-, the cross section could increase by 32% or decrease by 13%. In the case of associated production with a top quark pair $e^+e^- \to ht\bar{t}$, the cross section can be enhanced up to several times when the custodial triplet scalar H_3^0 is resonantly produced. In the meanwhile, the double Higgs production $e^+e^- \to hhZ$ ($hh\nu\bar{\nu}$) can be maximally enhanced by one order of magnitude at the resonant $H_{1,3}^0$ production. We also include exclusion limits expected from future LHC runs at higher energy and luminosity and discuss their further constraints on the relevant model parameters. We find that the GM model can result in likely measurable deviations of Higgs production from the SM at future e^+e^- colliders.

Keywords: Beyond Standard Model, Higgs Physics, Neutrino Physics

ArXiv ePrint: 1710.00184

[1] Current address: School of Physics, Peking University, Beijing 100871, China.

https://doi.org/10.1007/JHEP02(2018)007

JHEP02(2018)007

Contents

JHEP02(2018)007

1 Introduction

The discovery of a 125 GeV scalar at the Large Hadron Collider (LHC) [1, 2] confirmed the Higgs mechanism of electroweak symmetry breaking in the standard model (SM) [3–8]. Yet the sector that triggers the symmetry breaking remains to be disclosed. With an elementary scalar the SM is also confronted with issues such as gauge hierarchy and flavor problems. To solve or relax some of these issues, there have been various theoretical attempts beyond the SM whose phenomenologies have been extensively studied, such as in the minimal supersymmetric model (MSSM) [9–12], two Higgs doublet models (THDM) [13–18], little Higgs models [19–23], and composite Higgs models [24–26], to mention a few with a modified Higgs sector.

To unravel the symmetry breaking sector it is necessary to measure the interactions of the Higgs boson with itself and other related particles. While this is believed to be

very challenging at the LHC [27], future lepton colliders provide an avenue to study these interactions at a reasonably good precision due to cleaner environment [28]. There have been several proposals for next-generation e^+e^- colliders that are under active studies, including the Circular Electron-Positron Collider (CEPC) [29, 30], the Future Circular Collider (FCC-ee) [31], the Compact Linear Collider (CLIC) [32, 33], and the International Linear Collider (ILC) [34–36]. These colliders are planned to operate at a center of mass (CM) energy ranging from about 250 GeV to 3 TeV, thereby making accessible most of dominant production processes of the Higgs boson.

At an e^+e^- collider of high enough energy one could study simultaneously the interactions of the Higgs boson h with itself and with gauge bosons $W^\pm$, Z or even fermions such as the top quark t. This would be very helpful for us to build an overall picture on the symmetry breaking sector and gain a hint on possible physics that goes beyond the SM. The hZZ coupling can be measured via the Higgs-strahlung process $e^+e^- \to hZ$ and the ZZ fusion process $e^+e^- \to (ZZ \to h)e^+e^-$, while the hWW coupling can be probed via the WW fusion process $e^+e^- \to (WW \to h)\nu\bar{\nu}$. The top Yukawa coupling can possibly be extracted from the associated production process $e^+e^- \to ht\bar{t}$. And finally, the Higgs pair production processes $e^+e^- \to hh\nu\bar{\nu}$, hhZ provide an access to the trilinear coupling of the Higgs boson. These processes are generally modified by new interactions or new heavy particles, and precise measurements on them could help us identify the imprints of physics beyond the SM [37–53].

In this work we will study the above mentioned dominant single and double Higgs production at future e^+e^- colliders in the Georgi-Machacek (GM) model [54, 55]. The model is interesting because it introduces weak isospin-triplet scalars in a manner that preserves the custodial $\mathrm{SU}(2)_V$ symmetry. While this symmetry guarantees that the ρ parameter is naturally unity at the tree level, the arrangement of the triplet scalars allows them to develop a vacuum expectation value (VEV) as large as a few tens of GeV. After spontaneous symmetry breaking there remain ten physical scalars that can be approximately classified into irreducible representations of $\mathrm{SU}(2)_V$, one quintuplet, one triplet and two singlets. These multiplets couple to gauge bosons and fermions differently. In particular, the couplings of the SM-like Higgs boson h can be significantly modified, and processes involving h receive additional contributions from new scalars as intermediate states. It is a distinct feature of the GM model compared to a scalar sector with only singlet and doublet scalars that the h couplings to fermions and gauge bosons may be enhanced, or always enhanced in the case of the quartic couplings to a gauge boson pair.

The GM model has been extended by embedding it in more elaborate theoretical scenarios such as little Higgs [56, 57] and supersymmetric models [58, 59], by generalizing it to larger SU(2) multiplets [60] or including dark matter [61, 62]. The phenomenology of exotic scalars has previously been studied, including searches for exotic scalars and the application of a variety of constraints on the model parameter space [63–85]; in particular, previous works on e^+e^- colliders [75, 80] mainly concentrated on the custodial quintuplet particles. When these exotic scalars are heavy, it is difficult to produce them directly even at LHC, but we will show that they could be probed indirectly at e^+e^- colliders via modifications to the SM-like Higgs production processes. If the new scalars are light

JHEP02(2018)007

enough, they could contribute as resonances in those processes and thus affect them more significantly. In either case, high energy e^+e^- colliders could provide a viable way to test the GM model.

This paper is organized as follows. We recall in the next section the basic features in the Higgs sector of the Georgi-Machacek model. We discuss in section 3 various constraints on the model parameter space coming from current and future LHC runs as well as from low energy precision measurements and theoretical considerations. Then we investigate various SM-like Higgs production processes in section 4 at the 500 GeV and 1 TeV ILC. We reserve for our future work a comparative study of electron colliders operating at various energies and luminosities which requires a detailed simulation of the relevant processes. We finally summarize our main results in section 5. Some lengthy coefficients and Higgs trilinear couplings are delegated to appendices A, B, and C.

2 The Georgi-Machacek model

The model contains the usual Higgs doublet scalar ϕ with hypercharge $Y = 1/2$ and introduces a new complex triplet scalar χ with $Y = 1$ and a new real triplet scalar ξ with $Y = 0$. To make the custodial symmetry manifest, it is convenient to recast them in a matrix form:

$$\Phi = \begin{pmatrix} \phi^{0*} & \phi^+ \\ -\phi^- & \phi^0 \end{pmatrix}, \quad \Delta = \begin{pmatrix} \chi^{0*} & \xi^+ & \chi^{++} \\ -\chi^- & \xi^0 & \chi^+ \\ \chi^{--} & -\xi^- & \chi^0 \end{pmatrix}, \tag{2.1}$$

using the phase convention, $\chi^{--} = (\chi^{++})^*$, $\chi^- = (\chi^+)^*$, $\xi^- = (\xi^+)^*$, $\phi^- = (\phi^+)^*$, and $\xi^0 = (\xi^0)^*$. The matrices Φ and Δ transform under $\mathrm{SU}(2)_L \times \mathrm{SU}(2)_R$ as $\Phi \to U_L \Phi U_R^\dagger$ and $\Delta \to U_L \Delta U_R^\dagger$ with $U_{L,R} = \exp(i\theta^a_{L,R} T^a)$, where, for Φ, $T^a = \tau^a/2$ with τ^a being the Pauli matrices, and for Δ, $T^a = t^a$ are

$$t^1 = \frac{1}{\sqrt{2}} \begin{pmatrix} 0 & 1 & 0 \\ 1 & 0 & 1 \\ 0 & 1 & 0 \end{pmatrix}, \; t^2 = \frac{1}{\sqrt{2}} \begin{pmatrix} 0 & -i & 0 \\ i & 0 & -i \\ 0 & i & 0 \end{pmatrix}, \; t^3 = \begin{pmatrix} 1 & 0 & 0 \\ 0 & 0 & 0 \\ 0 & 0 & -1 \end{pmatrix}. \tag{2.2}$$

The most general scalar potential invariant under $\mathrm{SU}(2)_L \times \mathrm{SU}(2)_R \times \mathrm{U}(1)_Y$ is given by [86]

$$\begin{aligned} V_H = {} & \frac{1}{2}\mu_2^2 \mathrm{tr}(\Phi^\dagger\Phi) + \frac{1}{2}\mu_3^2 \mathrm{tr}(\Delta^\dagger\Delta) + \lambda_1[\mathrm{tr}(\Phi^\dagger\Phi)]^2 + \lambda_2 \mathrm{tr}(\Phi^\dagger\Phi)\mathrm{tr}(\Delta^\dagger\Delta) \\ & + \lambda_3 \mathrm{tr}(\Delta^\dagger\Delta\Delta^\dagger\Delta) + \lambda_4[\mathrm{tr}(\Delta^\dagger\Delta)]^2 - \lambda_5 \mathrm{tr}(\Phi^\dagger\tau^a\Phi\tau^b)\mathrm{tr}(\Delta^\dagger t^a \Delta t^b) \\ & - M_1 \mathrm{tr}(\Phi^\dagger\tau^a\Phi\tau^b)(U\Delta U^\dagger)_{ab} - M_2 \mathrm{tr}(\Delta^\dagger t^a \Delta t^b)(U\Delta U^\dagger)_{ab}, \end{aligned} \tag{2.3}$$

where all free parameters are real and the matrix U is [87]

$$U = \begin{pmatrix} -\frac{1}{\sqrt{2}} & 0 & \frac{1}{\sqrt{2}} \\ -\frac{i}{\sqrt{2}} & 0 & -\frac{i}{\sqrt{2}} \\ 0 & 1 & 0 \end{pmatrix}. \tag{2.4}$$

JHEP02(2018)007

The spontaneous symmetry breaking is triggered by the VEVs $\langle\Phi\rangle = 1_2 v_\phi/\sqrt{2}$ and $\langle\Delta\rangle = 1_3 v_\Delta$. As usual, the weak gauge bosons obtain masses from the kinetic terms of the scalars

$$\mathcal{L} = \frac{1}{2}\mathrm{tr}[(D^\mu\Phi)^\dagger D_\mu\Phi] + \frac{1}{2}\mathrm{tr}[(D^\mu\Delta)^\dagger D_\mu\Delta], \tag{2.5}$$

where

$$\begin{aligned} D_\mu\Phi &= \partial_\mu\Phi + ig_2 A^a_\mu \frac{\tau^a}{2}\Phi - ig_1 B_\mu \Phi\frac{\tau^3}{2}, \\ D_\mu\Delta &= \partial_\mu\Delta + ig_2 A^a_\mu t^a\Delta - ig_1 B_\mu \Delta t^3, \end{aligned} \tag{2.6}$$

with $g_{2,1}$ being the gauge couplings of $\mathrm{SU}(2)_L \times \mathrm{U}(1)_Y$. Their squared masses are $m_W^2 = g_2^2 v^2/4$ and $m_Z^2 = (g_1^2+g_2^2)v^2/4$ where

$$v^2 = v_\phi^2 + 8v_\Delta^2, \tag{2.7}$$

which should be identified with $1/(\sqrt{2}G_F)$ where G_F is the Fermi constant. The parameter $\rho = 1$ is thus established at the tree level. Since the custodial symmetry is explicitly broken by hypercharge and Yukawa couplings, divergent radiative corrections to ρ will generally appear at one loop within the framework of the GM model [88].

Restricting our discussions to the tree level, the custodial symmetry is respected by the scalar spectra so that the scalars can be classified into irreducible representations of $\mathrm{SU}(2)_V$. Excluding the would-be Nambu-Goldstone bosons to be eaten up by the weak gauge bosons, they are decomposed into a quintuplet, a triplet and two singlets. Denoting the real and imaginary parts of the neutral components of the original fields after extracting out the VEVs,

$$\phi^0 = \frac{1}{\sqrt{2}}(v_\phi + \phi^r + i\phi^i),\ \chi^0 = v_\Delta + \frac{1}{\sqrt{2}}(\chi^r + i\chi^i),\ \xi^0 = v_\Delta + \xi^r, \tag{2.8}$$

the quintuplet states are [86]

$$\begin{aligned} H_5^{++} &= \chi^{++}, \\ H_5^{+} &= \frac{1}{\sqrt{2}}(\chi^+ - \xi^+), \\ H_5^{0} &= \sqrt{\frac{2}{3}}\xi^r - \sqrt{\frac{1}{3}}\chi^r, \end{aligned} \tag{2.9}$$

plus $H_5^{--,-} = (H_5^{++,+})^*$. The triplet states are

$$\begin{aligned} H_3^+ &= -s_H\phi^+ + c_H\frac{1}{\sqrt{2}}(\chi^+ + \xi^+), \\ H_3^0 &= -s_H\phi^i + c_H\chi^i, \end{aligned} \tag{2.10}$$

plus $H_3^- = (H_3^+)^*$, where the doublet-triplet mixing angle θ_H is defined by

$$c_H \equiv \cos\theta_H = \frac{v_\phi}{v},\ s_H \equiv \sin\theta_H = \frac{2\sqrt{2}v_\Delta}{v}. \tag{2.11}$$

JHEP02(2018)007

We denote the quintuplet and triplet masses as m_5 and m_3 respectively. At the Lagrangian level, the quintuplet scalars couple to the electroweak gauge bosons but not to fermions (i.e., with H_5VV but without $H_5f\bar{f}$ couplings), while the opposite is true for the triplet scalars (with $H_3f\bar{f}$ but without H_3VV couplings).

The two custodial singlets mix by an angle α into the mass eigenstates

$$\begin{aligned} h &= c_\alpha \phi^r - s_\alpha \left(\sqrt{\frac{1}{3}}\xi^r + \sqrt{\frac{2}{3}}\chi^r \right), \\ H_1^0 &= s_\alpha \phi^r + c_\alpha \left(\sqrt{\frac{1}{3}}\xi^r + \sqrt{\frac{2}{3}}\chi^r \right), \end{aligned} \tag{2.12}$$

with $c_\alpha = \cos\alpha$ and $s_\alpha = \sin\alpha$. We assume that the lighter state h is the observed 125 GeV scalar [1, 2, 89]. The angle is determined by [86]

$$\sin 2\alpha = \frac{2M_{12}^2}{m_1^2 - m_h^2}, \quad \cos 2\alpha = \frac{M_{22}^2 - M_{11}^2}{m_1^2 - m_h^2}, \tag{2.13}$$

where $m_{h,1}$ are the masses of h and H_1^0 respectively, and in terms of the scalar couplings and VEVs,

$$\begin{aligned} M_{11}^2 &= 8\lambda_1 v_\phi^2, \\ M_{12}^2 &= \frac{\sqrt{3}}{2} v_\phi \left[-M_1 + 4(2\lambda_2 - \lambda_5) v_\Delta \right], \\ M_{22}^2 &= \frac{M_1 v_\phi^2}{4 v_\Delta} - 6 M_2 v_\Delta + 8(\lambda_3 + 3\lambda_4) v_\Delta^2. \end{aligned} \tag{2.14}$$

3 Constraints on parameter space

There are generally many free parameters in the scalar potential with an extended scalar sector. In this section, we will perform a combined analysis based on theoretical considerations and indirect and direct constraints to obtain the allowed regions for the parameters that are most relevant for our later Higgs production processes. The theoretical constrains are mainly derived from the requirement of perturbativity and vacuum stability [86, 87], while the indirect ones cover the oblique parameters (S, T, U), the Z-pole observables (R_b), and the B-meson observables [86, 90]. Among the B-meson observables ($B_s^0 - \bar{B}_s^0$ mixing, $B_s^0 \to \mu^+\mu^-$, and $b \to s\gamma$), the decay $b \to s\gamma$ currently sets the strongest bound. All of these constraints have been implemented in the calculator GMCALC [91] for the GM model, which will be applied as our starting point. On top of this we will impose up-to-date direct experimental constraints which cover the searches for a heavy neutral Higgs boson (H_1^0), custodial triplet bosons (H_3) and quintuplet bosons (H_5), and the signal strength analysis of the SM-like Higgs boson (h). For the signal strength analysis, we will also include the constraints expected from future runs of LHC and the proposed ILC. In figure 1 we show how survived points in the $\alpha - v_\Delta$ plane evolve with the inclusion of various constraints. With theoretical and indirect constraints alone, a v_Δ as large as 60 GeV is still allowed. When the constraints from direct searches for H_1^0 (black points),

JHEP02(2018)007

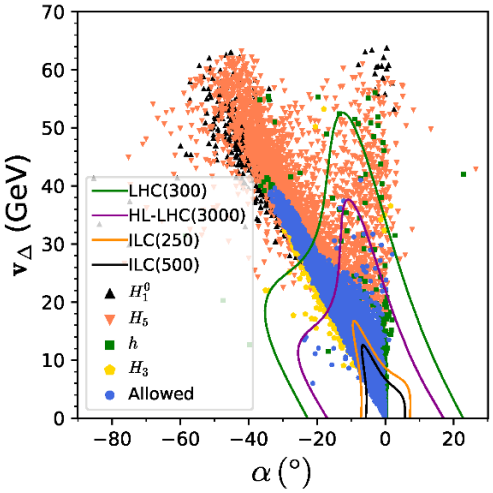

Figure 1. Distribution of survived points in the $\alpha - v_\Delta$ plane under theoretical and indirect constraints generated by GMCALC. The black, red, yellow, and green points are further excluded by direct searches for H_1^0, H_5, and H_3 and by Higgs signal strength analysis respectively, while the circular blue points pass all current constraints. The green, magenta, orange, and black curves are exclusion bounds expected from projection results of 14 TeV LHC with 300 fb^{-1}, HL-LHC with 3000 fb^{-1}, and ILC at 250 and 500 GeV.

H_5 (red), H_3 (yellow) and from the Higgs signal strength (green) are included, more and more points are excluded. At this stage, we have $v_\Delta \lesssim 40$ GeV, and $\alpha < 0$ is preferred. Also shown in the figure are the future prospects of constraints derived from Higgs signal strength measurements at 14 TeV LHC with 300 fb^{-1} (green curve), High-Luminosity LHC (HL-LHC) with 3000 fb^{-1} (magenta) [92], ILC with 1150 fb^{-1} at 250 GeV (orange) and 1600 fb^{-1} at 500 GeV (black) [35]. It is clear that a wide parameter space will be within the reach of future ILC operations. In the following subsections we will describe these direct experimental constraints in more detail.

3.1 Singlet searches

In the GM model, the heavy neutral Higgs boson H_1^0 can decay to a pair of vector bosons when it is above the threshold. Searches for heavy resonances decaying to a WW [93] and ZZ [94] pair are performed by the ATLAS Collaboration using the data collected at $\sqrt{s} = 13$ TeV with an integrated luminosity of 13.2 fb^{-1}. For the gluon fusion (ggF) and vector boson fusion (VBF) production of the heavy Higgs, the corresponding cross sections are calculated as

$$\begin{aligned}\sigma_{\rm ggF}^{\rm GM} &= \sigma_{\rm The}(gg \to H_1^0) \times \kappa^2_{H_1^0 f\bar{f}} \times {\rm BR}_{\rm GM}(H_1^0 \to VV),\\ \sigma_{\rm VBF}^{\rm GM} &= \sigma_{\rm The}(qq \to H_1^0) \times \kappa^2_{H_1^0 VV} \times {\rm BR}_{\rm GM}(H_1^0 \to VV),\end{aligned} \tag{3.1}$$

where

$$\begin{aligned}\kappa_{H_1^0 f\bar{f}} &\equiv \frac{g_{H_1^0 f\bar{f}}}{g^{\rm SM}_{hf\bar{f}}} = \frac{s_\alpha}{c_H},\\ \kappa_{H_1^0 VV} &\equiv \frac{g_{H_1^0 VV}}{g^{\rm SM}_{hVV}} = s_\alpha c_H + \frac{2\sqrt{6}}{3} c_\alpha s_H,\end{aligned} \tag{3.2}$$

JHEP02(2018)007

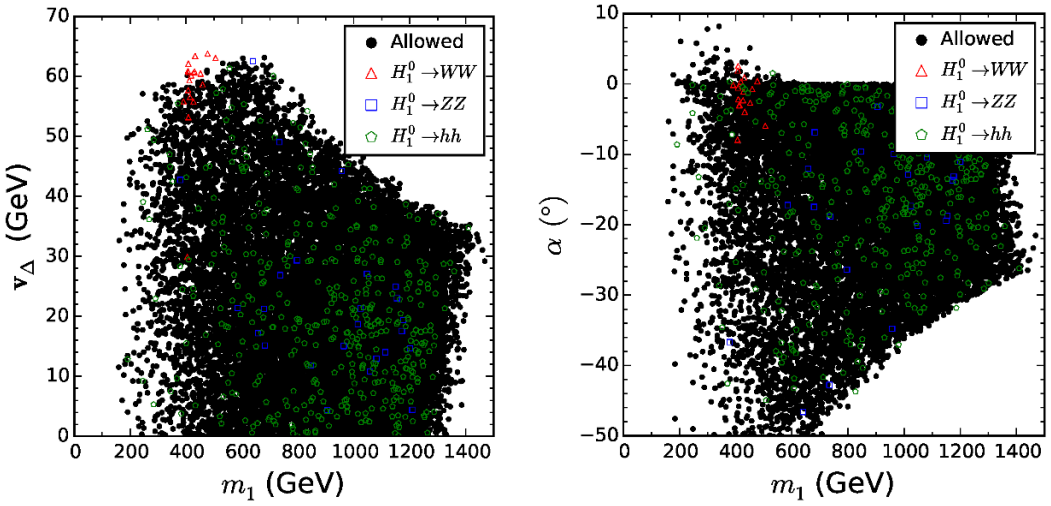

Figure 2. Distribution of survived points shown in the $v_\Delta - m_1$ plane (left) and $\alpha - m_1$ plane (right). The red, blue, and green points are excluded by the $H_1^0 \to WW,\ ZZ,\ hh$ searches respectively.

with gs denoting the couplings in the SM and the GM model. The theoretical cross sections of a SM-like heavy Higgs $\sigma_{\rm The}(gg \to H_1^0)$ and $\sigma_{\rm The}(qq \to H_1^0)$ have been tabulated in ref. [95], while the branching ratio $\mathrm{BR}_{\rm GM}(H_1^0 \to VV)$ is obtained using GMCALC.

When $m_1 > 2m_h$, H_1^0 can also decay into a Higgs pair hh, which may greatly enhance the Higgs pair production at the LHC. The cross section for resonant production of a Higgs boson pair is given by [96]

$$\sigma(pp \to H_1^0 \to hh) = \sigma_{\rm The}(gg \to H_1^0) \times \kappa^2_{H_1^0 f\bar{f}} \times \mathrm{BR}_{\rm GM}(H_1^0 \to hh), \tag{3.3}$$

where $\mathrm{BR}_{\rm GM}(H_1^0 \to hh)$ is also calculated by GMCALC. Recently, a search for resonant Higgs boson pair production ($H_1^0 \to hh$) has been performed by the CMS Collaboration [97] in the $b\bar{b}\ell\ell\nu\nu$ final state.

In figure 2 we show in the $v_\Delta - m_1$ and $\alpha - m_1$ planes the survived points upon applying the constraints from the direct searches $H_1^0 \to WW$, $H_1^0 \to ZZ$, and $H_1^0 \to hh$. While the $H_1^0 \to WW,\ ZZ$ searches remove only a small portion of points, a considerable portion is excluded by the $H_1^0 \to hh$ search. Due to large variations of $\mathrm{BR}(H_1^0 \to hh)$ in our scan [96], no clear dependence of the exclusion bounds on v_Δ and α is visible.

3.2 Triplet searches

The signature of a neutral triplet Higgs boson H_3^0 has been considered in ref. [98]. Without direct couplings to gauge bosons, the promising signature is $gg \to H_3^0 \to Zh$ for $m_Z + m_h < m_3 < 2m_t$, or $gg \to H_3^0 \to t\bar{t}$ for $m_3 > 2m_t$ [98]. The charged triplet Higgs boson H_3^+ can decay into $\tau^+\nu$ for $m_3 < m_t$ or into $t\bar{b}$ for $m_3 > m_t + m_b$ [67]. We therefore consider the following direct searches:

- Search for a CP-odd Higgs boson H_3^0 decaying to hZ [99, 100].
- Search for a heavy Higgs boson H_3^0 decaying to a top quark pair [101].

JHEP02(2018)007

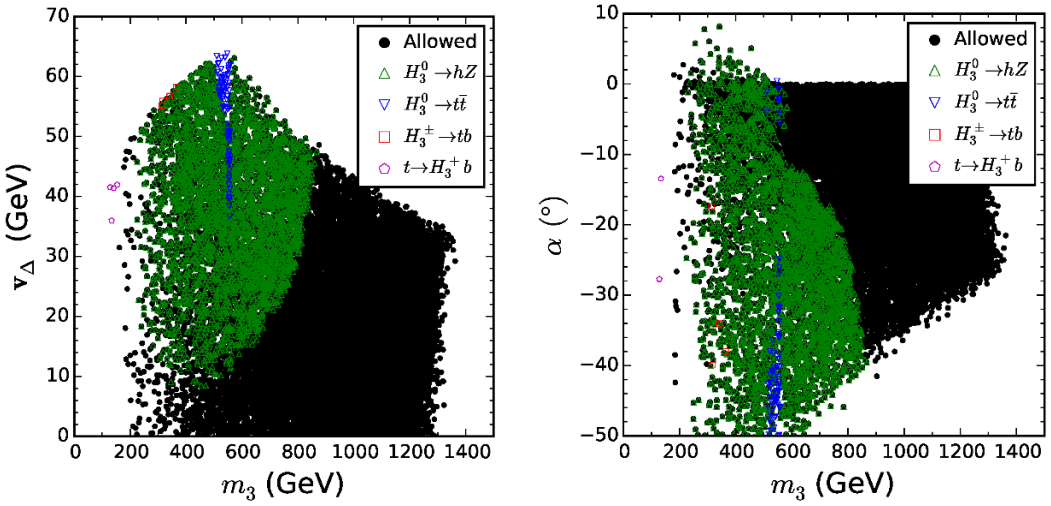

Figure 3. Distribution of survived points shown in the $v_\Delta - m_3$ plane (left) and $\alpha - m_3$ plane (right). The green, blue, red, and purple points are excluded by the $H_3^0 \to hZ$, $H_3^0 \to t\bar{t}$, $H^\pm \to tb$, and $t \to H_3^+ b$ searches respectively.

- Search for charged Higgs bosons decaying via $t \to H_3^+(\to \tau^+\nu)b$ or $H_3^\pm \to tb$ [102, 103].

Our results are shown in figure 3 in the $v_\Delta - m_3$ and $\alpha - m_3$ planes. Among the constraints from those searches, $H_3^0 \to hZ$ sets the most stringent one. In particular, in the mass region $200 \lesssim m_3 \lesssim 500$ GeV, where $\mathrm{BR}(H_3^0 \to hZ)$ is dominant or relatively large, v_Δ can be pushed down as low as 10 GeV under certain circumstances.

3.3 Quintuplet searches

Being independent of the singlet mixing angle α, the constraints on the quintuplet scalars are only sensitive to the VEV v_Δ and their mass m_5. In ref. [98] the constraint on v_Δ has been obtained as a function of the exotic Higgs boson mass via various channels for the additional neutral scalars in the GM model. In this paper, we adopt the constraints from the decay channels $H_5^0 \to \gamma\gamma$ and $H_5^0 \to ZZ$ through the VBF mechanism.

In refs. [104, 105] a search was performed for heavy charged scalars decaying to $W^\pm$ and Z bosons at $\sqrt{s} = 13$ TeV LHC. The upper limits on the cross section for the production of charged Higgs bosons times branching fractions to $W^\pm Z$ are transformed to the exclusion limits on v_Δ versus m_5 in the GM model.

The experimental constraints on the H_5^{++} mass were studied in the GM model in ref. [106] by recasting the ATLAS measurement of the cross section for the like-sign di-boson process $pp \to W^\pm W^\pm jj$. The $W^+W^+W^-W^-$ vertex is effectively modified by mediations of the doubly-charged Higgs bosons $H^{\pm\pm}$. That the relevant $W^\pm W^\pm H^{\mp\mp}$ vertex is proportional to v_Δ can be used to exclude parameter space on the plane of v_Δ and m_5. In this work we also take into account the latest search for like-sign W boson pairs by the CMS [107].

JHEP02(2018)007

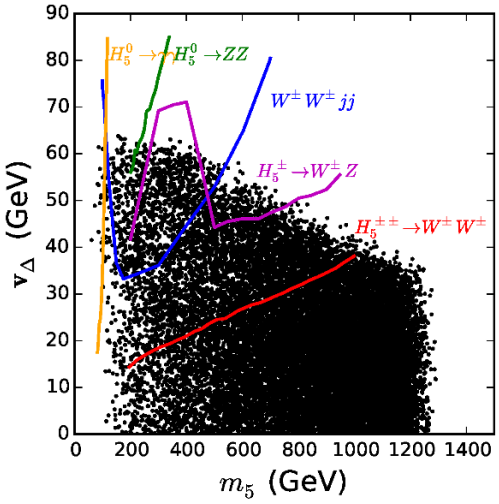

Figure 4. Constraints from searches for quintuplet Higgs bosons on the $v_\Delta - m_5$ plane. Points above exclusion curves are eliminated.

Additional subsidiary constraints are as follows:

- An absolute lower bound on the doubly-charged Higgs mass from the ATLAS like-sign dimuon data was obtained in ref. [108], which gives $m_5 \gtrsim 76\,\text{GeV}$.
- An upper bound on s_H for $m_5 \sim 76 - 100$ GeV can be obtained using the results of a decay-model-independent search for new scalars produced in association with a Z boson from the OPAL detector at the LEP collider [109].
- A limit $\tan\theta_H < 10/3$ is imposed to avoid a nonperturbative top quark Yukawa coupling [110].

In figure 4, we summarize the constraints from searches for quintuplet Higgs bosons on the $v_\Delta - m_5$ plane. In the low mass region 76 GeV $< m_5 <$ 110 GeV, the most stringent constraint comes from the neutral Higgs boson decay $H_5^0 \to \gamma\gamma$ through the VBF production. In the mass interval $110 - 200$ GeV, the like-sign diboson process $pp \to W^\pm W^\pm jj$ via the doubly-charged Higgs boson $H_5^{\pm\pm}$ gives the best bound. Above 200 GeV, the most severe constraint is set by the latest search for like-sign W boson pairs, which could exclude $v_\Delta \gtrsim 15$ GeV when $m_5 \sim 200$ GeV.

3.4 Higgs signal strengths

The signal strengths of the SM-like Higgs boson production and decay in various channels can provide significant constraints on its couplings to the SM particles in the GM model [111]. The signal strength for a specific production and decay channel $i \to h \to f$ is defined as

$$\mu_i^f = \frac{\sigma_i \times \text{BR}_f}{\sigma_i^{\text{SM}} \times \text{BR}_f^{\text{SM}}}, \tag{3.4}$$

where σ_i (σ_i^{SM}) is the reference value (SM prediction) of the Higgs production cross section for $i \to h$, and BR_f (BR_f^{SM}) the branching ratio for the decay $h \to f$. We include

JHEP02(2018)007

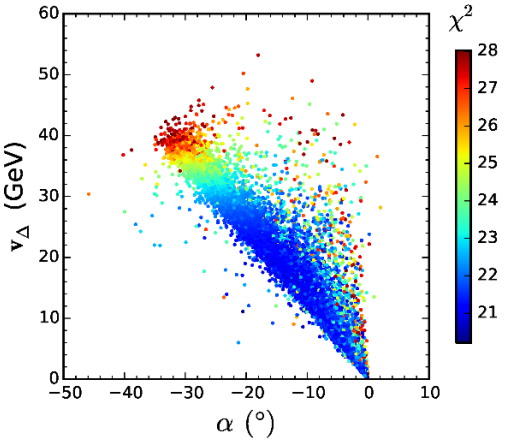

Figure 5. Scatter plot of the Higgs signal strength χ^2 fit with a 2σ range shown in the $\alpha - v_\Delta$ plane.

the production channels via the gluon fusion (ggF), the vector boson fusion (VBF), the associated production with a vector boson (Vh) and with a pair of top quarks (tth), and the decay channels $h \to \gamma\gamma$, ZZ, $W^\pm W^\mp$, $\tau^\pm\tau^\mp$, $b\bar{b}$. With the experimental values of $\mu_X^{\rm exp}$ and standard deviation $\Delta\mu_X^{\rm exp}$ [112], we build a χ^2 value for each allowed point as

$$\chi^2 = \sum_X \left(\frac{\mu_X^{\rm exp} - \mu_X}{\Delta\mu_X^{\rm exp}} \right)^2 , \tag{3.5}$$

where the sum extends over all channels mentioned above.

From eqs. (4.1), (4.6), we are aware that the SM-like Higgs couplings involved in the signal strengths depend only on the triplet VEV (v_Δ) and the singlet mixing angle (α). Therefore the constraints on v_Δ and α can be directly extracted from data without specifying other parameters. In figure 5 we show the scatter plot of χ^2 values on the $\alpha - v_\Delta$ plane within a 2σ range. It is clear that the measurement of the Higgs signal strengths is most sensitive to the region with large v_Δ and large $|\alpha|$, where large deviations of Higgs couplings from the SM take place. Hence the large χ^2 region, e.g., $v_\Delta \sim 50\,\text{GeV}$ and $\alpha \sim -40°$ would be excluded by future operations of LHC [76].

3.5 Future experimental constraints

For completeness we also presented in figure 1 the constraints of the Higgs signal strength χ^2 fit on the $\alpha - v_\Delta$ plane based on the projection results from 14 TeV LHC with an integrated luminosity of 300 fb^{-1} (LHC@300) and 3000 fb^{-1} (HL-LHC@3000) [92] and from ILC with an integrated luminosity of 1150 fb^{-1} at 250 GeV (ILC250) and 1600 fb^{-1} at 500 GeV (ILC500) [35]. The LHC (HL-LHC) result is performed on the ATLAS detector with only statistical and experimental systematic uncertainties taken into account. The expected precision is given as the relative uncertainty in the signal strength with the central values all assumed to be unity. In principle, this assumption applies only to the SM, but we employ these anticipated results as a reference so that we could be clear to what extent they can impose a constraint on the parameter space. It is clear from figure 1 that the constrains from LHC@300, HL-LHC@300, ILC250, and ILC500 gradually become more and

JHEP02(2018)007

more stringent. Basically speaking, the deviations in Higgs couplings are determined by α and v_Δ. Our fitting results show that LHC@300 (HL-LHC@3000) could approximately exclude $v_\Delta \gtrsim 30$ (20) GeV while ILC250 and ILC500 could further push it down to about $v_\Delta \gtrsim 10$ GeV.

Let us consider the scale factors κ_{hVV} and $\kappa_{hf\bar{f}}$ as an example under the assumption that no obvious deviations in Higgs couplings from SM values will be observed. At LHC@300, κ_{hVV} and $\kappa_{hf\bar{f}}$ could be constrained within the ranges $[0.92, 1.08]$ and $[0.93, 1.13]$ respectively, while at LHC@3000 they could be further narrowed down to $\kappa_{hVV} \in [0.97, 1.04]$ and $\kappa_{hf\bar{f}} \in [0.93, 1.06]$. At e^+e^- colliders, e.g., ILC, precision measurements of the Higgs productions and decays can rigorously constrain the parameter space. At ILC250 where $e^+e^- \to hZ$ dominates, measurements of the Higgs signal strength in this channel could give $\kappa_{hVV} \in [0.998, 1.02]$ and $\kappa_{hf\bar{f}} \in [0.995, 1.007]$. And at ILC500 measurements via the $e^+e^- \to hZ$ and $e^+e^- \to h\nu_e\bar{\nu}_e$ channels would yield $\kappa_{hVV} \in [0.998, 1.01]$ and $\kappa_{hf\bar{f}} \in [0.998, 1.004]$. On the other hand, if the on-going LHC observes a certain hint of Higgs coupling deviation , for instance, $\kappa_{hVV} > 1$ for the most optimistic case, the future operation of ILC will be hopeful to confirm it. In this way, the GM model would be strongly favored by the deviation $\kappa_{hVV} > 1$.

4 Higgs production at e^+e^- colliders

In this section we will study the dominant single and double SM-like Higgs production at future e^+e^- colliders in the GM model. For comparison we first reproduce in figure 6 the dominant Higgs production cross sections in the SM. The Higgs-strahlung (HS) process ($e^+e^- \to hZ$) is dominant for a CM energy $\sqrt{s} < 500$ GeV. At higher energy, the Higgs production is dominated by the WW fusion process ($e^+e^- \to h\nu_e\bar{\nu}_e$), while the ZZ fusion process ($e^+e^- \to he^+e^-$) also becomes significant. The subdominant processes such as $e^+e^- \to ht\bar{t}$, $e^+e^- \to hhZ$ and $e^+e^- \to hh\nu_e\bar{\nu}_e$ provide access to the top Yukawa coupling and the Higgs trilinear self-coupling.

It is clear that due to the s-channel topology (see figures 7, 10, 14), the hZ, $ht\bar{t}$, and hhZ production cross sections become maximal near the thresholds and decrease as collision energy goes up. On the contrary, the VBF ($h\nu_e\bar{\nu}_e$, he^+e^-, and $hh\nu_e\bar{\nu}_e$) cross sections increase as $\ln\sqrt{s}$ due to their t-channel topology (see figures 7, 16). These dominant processes can be divided into three types according to the couplings involved, namely the Higgs couplings to gauge bosons (figure 7) and to the top quark (figure 10), and the trilinear Higgs self-couplings (figures 14, 16), which we now investigate in detail for the GM model.

4.1 Production via Higgs-strahlung and vector boson fusion

In figure 7 we depict the Feynman diagrams for single Higgs production at e^+e^- colliders that involves only Higgs couplings to weak gauge bosons. The amplitudes for both HS and VBF processes are modified in the GM model by the same ratio of the Higgs-gauge couplings from the SM,

$$\kappa_{hVV} = \frac{g_{hVV}}{g_{hVV}^{\rm SM}} = c_\alpha c_H - \frac{2\sqrt{6}}{3} s_\alpha s_H, \tag{4.1}$$

JHEP02(2018)007

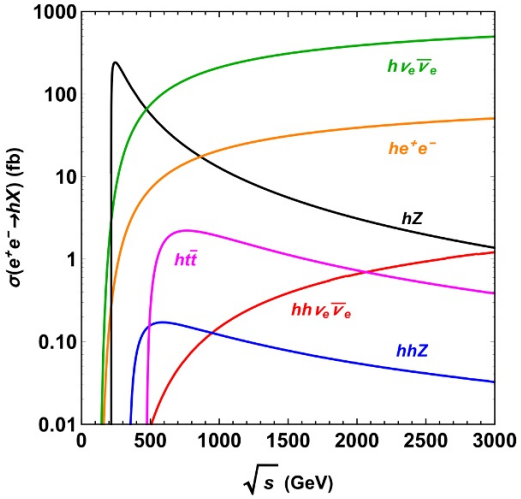

Figure 6. Cross section as a function of CM energy for dominant Higgs production processes in the SM at e^+e^- colliders with $m_h = 125\,\text{GeV}$.

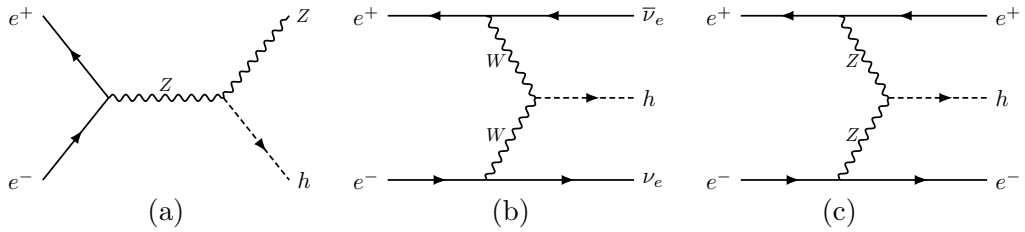

Figure 7. Feynman diagrams for Higgs production via HS (a) and VBF (b, c) at e^+e^- colliders.

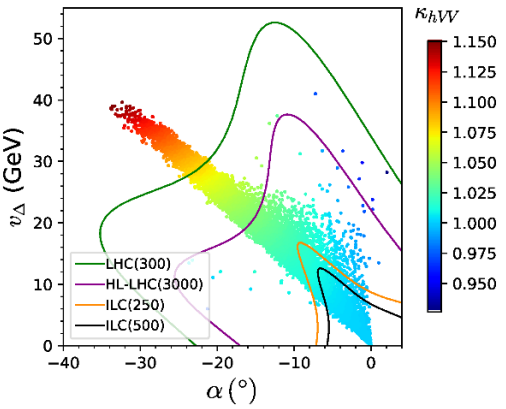

Figure 8. Predicted value of κ_{hVV} in the $v_\Delta - \alpha$ plane after imposing all the constraints in section 3.

where c_H and s_H are defined in eq. (2.11) in terms of v_Δ. We can thus extract κ^2_{hVV} by measuring these cross sections and set constraints on the parameters v_Δ and α,

The predicted value of κ_{hVV} in the $v_\Delta - \alpha$ plane is shown in figure 8. It is obvious that an $\mathcal{O}(10\%)$ deviation of κ_{hVV} from unity is still viable. Although the allowed κ_{hVV} is in a range of about 0.93-1.15, most of the survived points tend to have $\kappa_{hVV} > 1$. The

JHEP02(2018)007

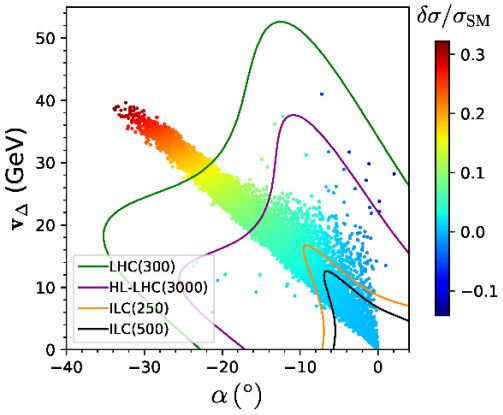

Figure 9. Distribution of relative corrections $\delta\sigma/\sigma_{\rm SM}$ in the $v_\Delta - \alpha$ plane for HS and VBF processes.

LHC@300 will mostly exclude $\kappa_{hVV} \gtrsim 1.1$, while HL-LHC@3000 could probe down to $\kappa_{hVV} \gtrsim 1.05$. The scale factor κ_{hVV} is expected to be measured at future e^+e^- colliders with high precision. For example, the measurements for the hVV couplings may reach an accuracy of 1% at CEPC (250 GeV, 5 ab^{-1}) and ILC (500 GeV, 500 fb^{-1}) [30, 35]. Hence, the GM model could be probed indirectly if a large enough deviation of κ_{hVV} from unity is measured. Especially, a measured $\kappa_{hVV} > 1$ would be strong evidence in favor of the GM model. If κ_{hVV} turns out to be consistent with unity, a precise measurement of it would put a stringent bound on the GM model parameter space.

The cross section for the HS process is [113]

$$\sigma(e^+e^- \to Zh) = \frac{G_F^2 m_Z^4}{96\pi s}(V_e^2 + A_e^2)\frac{\sqrt{\beta}(\beta + 12r_Z)}{(1-r_Z)^2}\kappa_{hVV}^2, \tag{4.2}$$

where the Z couplings to the fermion f of electric charge Q_f are $V_f = 2I_3^f - 4Q_f s_W^2$, $A_f = 2I_3^f$, with $I_3^f = \pm 1/2$ being the third weak isospin of the left-handed fermion f, and $s_W^2 = \sin^2\theta_W$ with θ_W being the Weinberg angle. And $\beta = (1 - r_Z - r_h)^2 - 4r_Z r_h$ is the usual two-body phase space function with $r_{h,Z,W} \equiv m_{h,Z,W}^2/s$, etc.

The total cross section for the WW (ZZ) fusion process is [114]

$$\sigma_{VV} = \frac{G_F^3 m_V^4}{64\sqrt{2}\pi^3}\int_{r_h}^1 dx \int_x^1 dy \frac{(V_V^2 + A_V^2)^2 f(x,y) + 4V_V^2 A_V^2 g(x,y)}{[1 + (y-x)/r_V]^2}\kappa_{hVV}^2, \tag{4.3}$$

where V denotes either W or Z, $V_W = A_W = \sqrt{2}$ ($V_Z = V_e$, $A_Z = A_e$) for the WW (ZZ) fusion respectively, and

$$f(x,y) = \left(\frac{2x}{y^3} - \frac{1+2x}{y^2} + \frac{2+x}{2y} - \frac{1}{2}\right)\left[\frac{z}{1+z} - \ln(1+z)\right] + \frac{x}{y^3}\frac{z^2(1-y)}{1+z}, \tag{4.4}$$

$$g(x,y) = \left(-\frac{x}{y^2} + \frac{2+x}{2y} - \frac{1}{2}\right)\left[\frac{z}{1+z} - \ln(1+z)\right], \tag{4.5}$$

with $z = y(x - r_h)/(xr_V)$.

The HS and VBF processes are within the reach of all future e^+e^- colliders mentioned in section 1. Their cross sections are corrected by the same factor of κ_{hVV}^2, so that their

JHEP02(2018)007

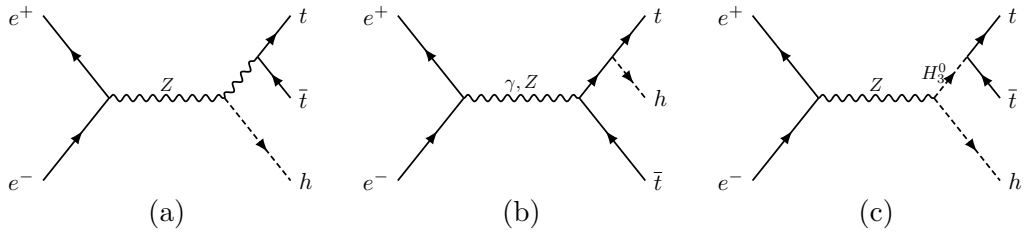

Figure 10. Feynman diagrams for $ht\bar{t}$ production at e^+e^- colliders.

relative corrections compared to the SM $\delta\sigma/\sigma_{\rm SM} = \kappa^2_{hVV} - 1$ are the same and independent of the collision energy. From figure 9, we see that the cross sections could maximally increase by 32% or decrease by 13% with the current constraints. Even if no clear deviation would be found at LHC@300 or HL-LHC@3000, an increase of up to 10% in the HS and VBF cross section would still be possible at the ILC.

4.2 Associated production with top quarks

The associated Higgs production with a top quark pair is an important process to measure the top quark Yukawa coupling at a linear collider [115–117]. Compared to the SM case, the existing interactions are modified and in addition there is a new contribution in the GM model that is mediated by the CP-odd heavy Higgs H_3^0, see figure 10. The scale factor to the SM $h\bar{f}f$ coupling is, $\kappa_{hf\bar{f}} = c_\alpha/c_H$, and those involving the custodial triplet H_3 are

$$\begin{aligned} -\kappa_{H_3^0 d\bar{d}} &= \kappa_{H_3^0 u\bar{u}} = \tan\theta_H, \\ \kappa_{H_3^0 hZ} &= \kappa_{H_3^+ hW^-} = c_\alpha s_H + \frac{2\sqrt{6}}{3} s_\alpha c_H, \end{aligned} \tag{4.6}$$

which appear in the Feynman rules as follows:

$$\begin{aligned} H_3^0 \bar{f} f &: \kappa_{H_3^0 f\bar{f}} \frac{m_f}{v} \gamma_5, \\ H_3^0 h Z^\mu &: \kappa_{H_3^0 hZ} \frac{e}{2 s_W c_W} (p_h - p_3)_\mu, \\ H_3^- h W^{+\mu} &: -i\kappa_{H_3^+ hW^-} \frac{e}{2 s_W} (p_h - p_3)_\mu, \end{aligned} \tag{4.7}$$

where p_h (p_3) is the incoming momentum of h ($H_3^{0,+}$). The scanned results for these κs are shown in figure 11 in the $v_\Delta - \alpha$ plane. For the current constraints, we see that a deviation from unity as large as $\mathcal{O}(\pm 10\%)$ is still allowed for $\kappa_{hf\bar{f}}$. The scale factor $\kappa_{H_3^0 f\bar{f}}$ does not depend on α, and its magnitude can maximally reach about 0.54 and vanishes in the limit of $v_\Delta \to 0$, while $\kappa_{H_3^0 hZ}$ lies in the interval of -0.2 to 0.6. The future operation of LHC@300 will be capable of excluding points with $\kappa_{hf\bar{f}} \lesssim 0.975$ and $|\kappa_{H_3^0 f\bar{f}}| \gtrsim 0.35$, while ILC500 has the ability to constrain $\kappa_{hf\bar{f}} \approx 1$, $|\kappa_{H_3^0 f\bar{f}}| \lesssim 0.1$, and $\kappa_{H_3^0 hZ} \in [0, 0.2]$.

JHEP02(2018)007

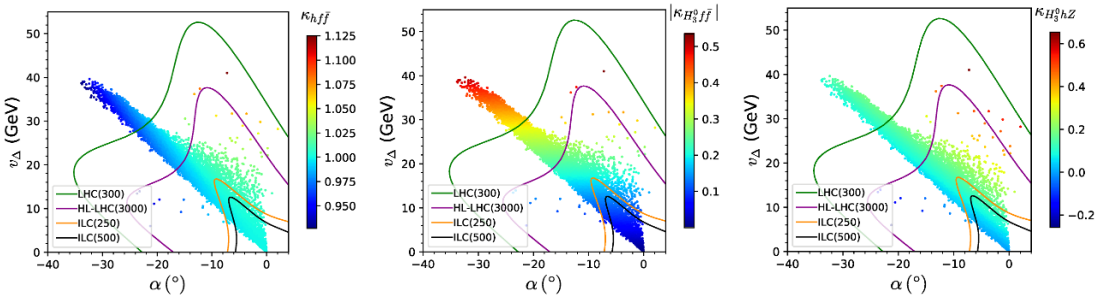

Figure 11. Predicted values of $\kappa_{hf\bar{f}}$, $|\kappa_{H_3^0 f\bar{f}}|$, and $\kappa_{H_3^0 hZ}$ in the $v_\Delta - \alpha$ plane after imposing all the constraints in section 3.

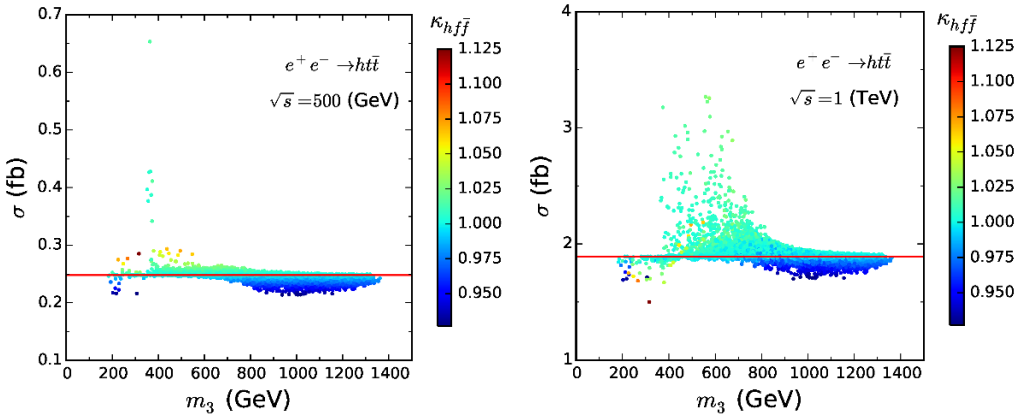

Figure 12. Cross section for $e^+e^- \to ht\bar{t}$ as a function of the H_3^0 mass m_3 at $\sqrt{s} = 500$ GeV (left) and 1000 GeV (right). The horizontal line indicates the SM result.

The cross section in the GM model can be adapted from those in the SM and MSSM [116, 117]

$$\frac{d\sigma(e^+e^- \to ht\bar{t})}{dx_h} = N_c \frac{\sigma_0}{(4\pi)^2} \Bigg\{ \Big[Q_e^2 Q_t^2 + \frac{2Q_e Q_t V_e V_t}{16 c_W^2 s_W^2 (1-r_Z)} + \frac{(V_e^2+A_e^2)(V_t^2+A_t^2)}{256 c_W^4 s_W^4 (1-r_Z)^2} \Big] G_1 + \frac{V_e^2+A_e^2}{256 c_W^4 s_W^4 (1-r_Z)^2} \Big[A_t^2 \sum_{i=2}^{6} G_i + V_t^2 (G_4+G_6) \Big] + \frac{Q_e Q_t V_e V_t}{1-r_Z} G_6 + G_7 \Bigg\}. \tag{4.8}$$

Here $\sigma_0 = 4\pi\alpha_{\rm QED}^2/(3s)$, $\alpha_{\rm QED}$ is the fine structure constant, $N_c = 3$, $x_h = 2E_h/\sqrt{s}$ with E_h the Higgs boson energy. The explicit expressions for the coefficients $G_i (i = 1, \cdots 7)$ are given in appendix A.

In figure 12 we present the cross section for $e^+e^- \to ht\bar{t}$ as a function of the H_3^0 mass m_3 at $\sqrt{s} = 500,\ 1000$ GeV. In the parameter region $2m_t < m_3 < \sqrt{s} - m_h$, the subprocess $e^+e^- \to hH_3^0$, $H_3^0 \to t\bar{t}$ is resonant, where the cross section can be strongly enhanced by several times. When the mass of H_3^0 is far above the resonant region, the cross section reduces gradually to the SM value. Interestingly, in the resonant region with enhanced cross section, we actually have $\kappa_{hf\bar{f}} \gtrsim 1$ for most of the survived points, while above this region the cross section decreases with the decrease of $\kappa_{hf\bar{f}}$. Combined with

JHEP02(2018)007

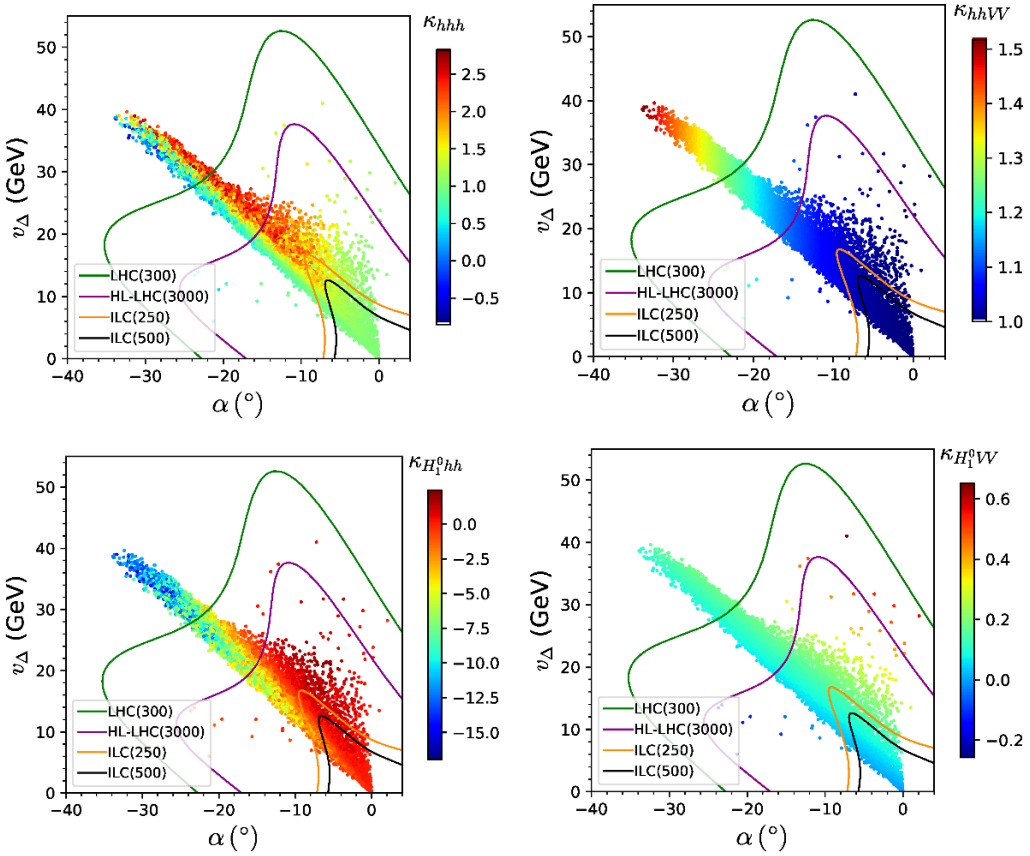

Figure 13. Same as figure 11, but for κ_{hhh}, κ_{hhVV}, $\kappa_{H_1^0hh}$ and $\kappa_{H_1^0VV}$

figure 11, most of points with $\kappa_{hf\bar{f}} < 1$ will be excluded by LHC@300 and HL-LHC@3000. Hence, large decrease of the $ht\bar{t}$ production might not be possible. On the other hand, for H_3^0 resonantly produced, most of allowed points actually have $\kappa_{hf\bar{f}} \approx 1$. Therefore, even if no large deviation in the Higgs coupling is observed at ILC250 or ILC500, significant enhancement of the $ht\bar{t}$ production may still be viable. At CLIC the expected accuracy for cross section is about 8.4% with an integrated luminosity of 1.5 ab^{-1} at $\sqrt{s} = 1.4$ TeV [33], and at ILC the accuracy could reach 28% (6.3%) at 500 (1000) GeV [35]. There is thus a good chance to test the $ht\bar{t}$ production at these high energy machines.

4.3 Double Higgs production

To study the Higgs self-interactions in the symmetry breaking sector, it is indispensable to measure the Higgs pair production at future e^+e^- colliders. In this subsection we consider possible production mechanisms in the GM model. These processes include the double Higgs-strahlung process $e^+e^- \to hhZ$ in figure 14 and the Higgs pair production via the W boson fusion $e^+e^- \to hh\nu_e\bar{\nu}_e$ in figure 16 while ignoring the much smaller Z boson fusion [33, 34]. These processes involve the scale factors

$$\kappa_{hhVV} = 1 + \frac{5}{3}s_\alpha^2, \tag{4.9}$$

JHEP02(2018)007

$\kappa_{H_1^0VV}$ shown in eq. (3.2), and $\kappa_{hhh} = g_{hhh}/g_{hhh}^{\rm SM}$, $\kappa_{H_1^0hh} = g_{H_1^0hh}/g_{hhh}^{\rm SM}$, where $g_{hhh}^{\rm SM} = 3m_h^2/v$, and g_{hhh}, $g_{H_1^0hh}$ are given in appendix B. In figure 13, we show the scanned results for these scale factors in the allowed parameter space. Compared to their SM counterparts, the $hhVV$ coupling is always enhanced due to $\kappa_{hhVV} \geq 1$, whereas the hhh coupling can even change its sign. For those points with $\kappa_{hhh} < 0$, LHC@300 will exclude most of them while HL-LHC@3000 could eliminate them altogether. The precision expected to be reachable at the ILC for the measurement of g_{hhh} is of $\mathcal{O}(10\%)$ [36], so the effect of the GM model should be observable. For the new couplings involving H_1^0, the magnitude of $\kappa_{H_1^0hh}$ can be so large that the processes are significantly enhanced but perturbation theory may not apply there, while the scale factor $\kappa_{H_1^0VV}$ ranges from -0.2 to 0.6. Considering the limit expected to be available at LHC@300 (HL-LHC@3000), $\kappa_{H_1^0hh} \lesssim 10$ ($\kappa_{H_1^0hh} \lesssim 5$) should be satisfied.

4.3.1 Double Higgs-Strahlung

The differential cross section for the process $e^+e^- \to hhZ$ can be written as [118–120]

$$\frac{d\sigma(e^+e^- \to hhZ)}{dx_1 dx_2} = \frac{G_F^3 m_Z^6}{384\sqrt{2}\pi^3 s}(V_e^2 + A_e^2)\frac{\mathcal{A}}{(1-r_Z)^2}. \tag{4.10}$$

In the above equation, $x_{1,2} = 2E_{1,2}/\sqrt{s}$ with $E_{1,2}$ being the energies of the Higgs bosons, and the shortcuts $x_3 = 2 - x_1 - x_2$, $y_i = 1 - x_i$ $(i = 1, 2, 3)$, $r_{1,3} = m_{1,3}^2/s$ are used. The function $\mathcal{A}$ can be expressed in the form [119]

$$\mathcal{A} = r_Z \left\{ \frac{1}{2}|a|^2 f_a + |b(y_1)|^2 f_b + 2\mathrm{Re}[ab^*(y_1)]g_{ab} + \mathrm{Re}[b(y_1)b^*(y_2)]g_{bb} \right\} + \{x_1, y_1 \leftrightarrow x_2, y_2\}, \tag{4.11}$$

where

$$\begin{aligned} a = &\frac{1}{2}\left(\frac{\kappa_{hVV}\kappa_{hhh}}{y_3 + r_Z - \tilde{r}_h} + \frac{\kappa_{H_1^0VV}\kappa_{H_1^0hh}}{y_3 + r_Z - \tilde{r}_1}\right)\frac{3m_h^2}{m_Z^2} \\ &+ \left(\frac{\kappa_{hVV}^2}{y_1 + r_h - \tilde{r}_Z} + \frac{\kappa_{hVV}^2}{y_2 + r_h - \tilde{r}_Z}\right) + \frac{\kappa_{hhVV}}{2r_Z}, \end{aligned} \tag{4.12}$$

$$b(y) = \frac{1}{2r_Z}\left(\frac{\kappa_{hVV}^2}{y + r_h - \tilde{r}_Z} + \frac{\kappa_{H_3^0hZ}^2}{y + r_h - \tilde{r}_3}\right). \tag{4.13}$$

Here $\tilde{r}_i$ $(i = h, Z, H_1, H_3)$ includes the total decay width of the particle i in its mass squared, i.e., $\tilde{r}_i = (m_i^2 - im_i\Gamma_i)/s$ when a resonance is crossed over. The coefficients f and g in eq. (4.11) are

$$\begin{aligned} f_a &= x_3^2 + 8r_Z, \\ f_b &= (x_1^2 - 4r_h)[(y_1 - r_Z)^2 - 4r_Z r_h], \\ g_{ab} &= r_Z[2(r_Z - 4r_h) + x_1^2 + x_2(x_2 + x_3)] - y_1(2y_2 - x_1x_3), \\ g_{bb} &= (y_3 - x_1x_2 - x_3r_Z - 4r_hr_Z)(2y_3 - x_1x_2 - 4r_h + 4r_Z) \\ &\quad + r_Z^2(4r_h + 6 - x_1x_2) + 2r_Z(r_Z^2 + y_3 - 4r_h). \end{aligned} \tag{4.14}$$

JHEP02(2018)007

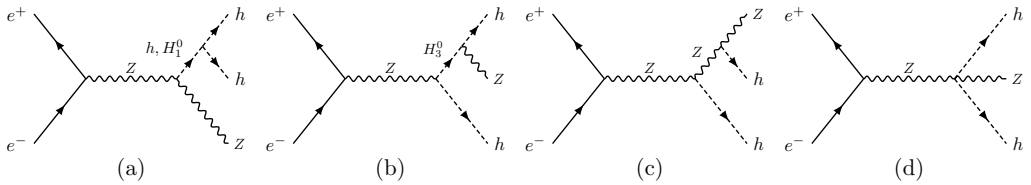

Figure 14. Feynman diagrams for hhZ production at e^+e^- colliders.

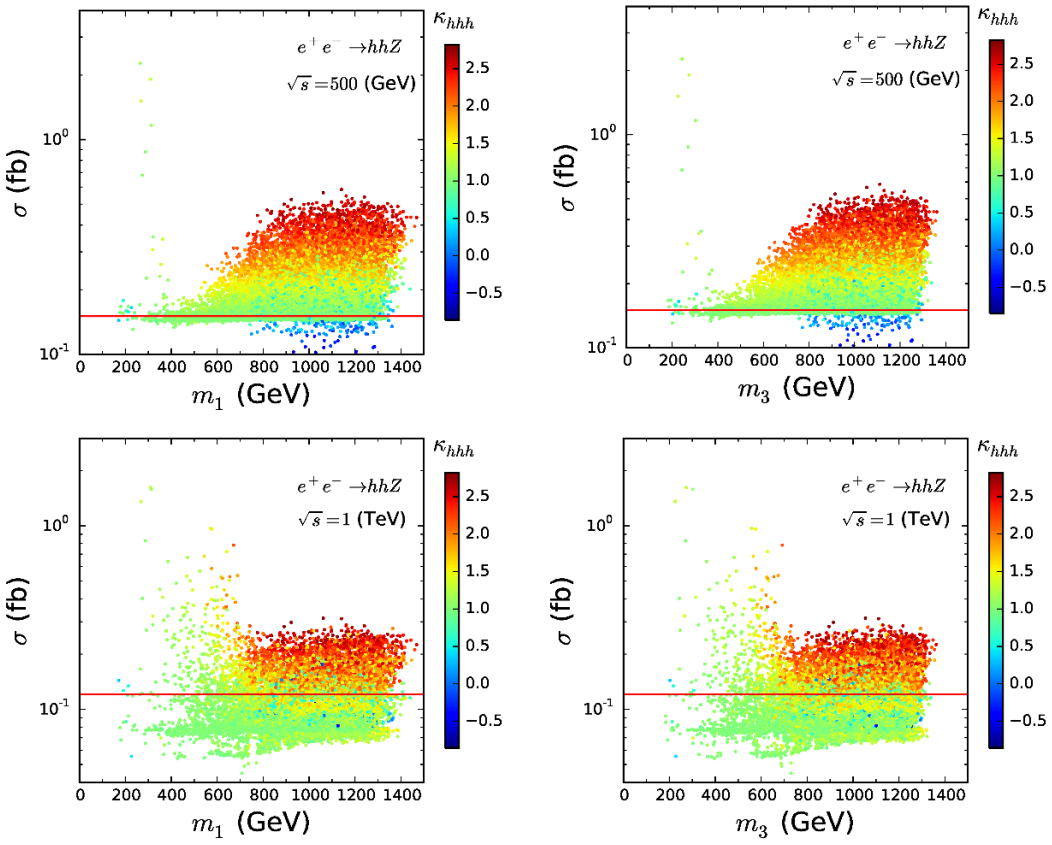

Figure 15. Cross section for $e^+e^- \to hhZ$ as a function of the H_1^0 mass m_1 (left panel) and H_3^0 mass m_3 (right) at $\sqrt{s} = 500$ GeV (upper) and 1 TeV (lower). The horizontal line indicates the SM value.

The double Higgs boson production is sensitive to the triple Higgs coupling g_{hhh}, which cannot be probed by the single Higgs boson production. In addition, the heavy CP-even Higgs boson H_1^0 contributes, thereby enabling sensitivity to the H_1^0hh coupling as well. The total cross section is shown in figure 15 at the energy $\sqrt{s} = 500$ GeV and 1 TeV. Compared to the SM case, the on-shell production of heavy scalars H_1^0 and H_3^0 followed by decays $H_1^0 \to hh$ and $H_3^0 \to hZ$ plays a dominant role in the resonant region of the parameter space, where the cross section can increase by more than one order of magnitude. Since in the resonance region, most of the currently allowed points have $\kappa_{hhh} \approx 1$, the future measurements at LHC@300 and HL-LHC@3000 would be hard to exclude such points. In the non-resonance region, the cross section at $\sqrt{s} = 500$ GeV is positively correlated with

JHEP02(2018)007

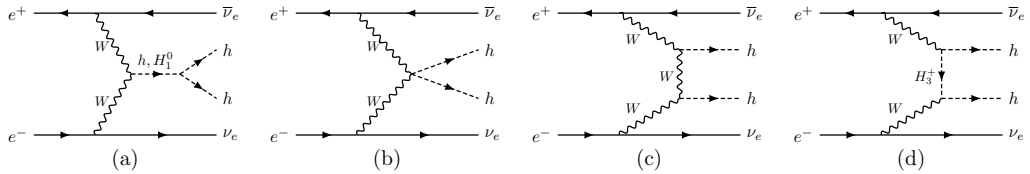

Figure 16. Feynman diagrams for double Higgs production from WW fusion at e^+e^- colliders.

κ_{hhh}, leading to enhanced cross section with $\kappa_{hhh} > 1$ or suppressed cross section with $\kappa_{hhh} < 1$. The cross section at $\sqrt{s} = 1$ TeV can be either enhanced or suppressed even with $\kappa_{hhh} \approx 1$.

4.3.2 Double Higgs from vector boson fusion

Besides the resonant WW fusion for single h production, there exists non-resonant WW fusion production of a pair of h, $e^+e^- \to hh\nu_e\bar{\nu}_e$, shown in figure 16. The GM model modifies existing interactions in the SM and introduces new contributions due to H_1^0 and $H_3^\pm$ exchanges. The cross section in the effective W approximation can be written as [119, 120]

$$\sigma(e^+e^- \to hh\nu_e\bar{\nu}_e) = \int_{x_{\min}}^1 dx \frac{dL}{dx}\hat{\sigma}_{WW}(x), \tag{4.15}$$

where $x_{\min} = 4r_h (= 4m_h^2/s)$, the differential luminosity function is [119]

$$\frac{dL(x)}{dx} = \frac{G_F^2 m_W^4}{8\pi^4}\frac{1}{x}[-(1+x)\ln x - 2(1-x)], \tag{4.16}$$

and the cross section for the subprocess is [119]

$$\begin{aligned}\hat{\sigma}_{WW}(x) = \frac{G_F^2\hat{s}}{64\pi}\Bigg[&4\beta_h\left(\frac{3r_h\kappa_{hVV}\kappa_{hhh}}{1-r_h} + \frac{3r_h\kappa_{H_1^0VV}\kappa_{H_1^0hh}}{1-r_1} + \kappa_{hhVV}\right)^2 \\ &+ 2\left(\frac{3r_h\kappa_{hVV}\kappa_{hhh}}{1-r_h} + \frac{3r_h\kappa_{H_1^0VV}\kappa_{H_1^0hh}}{1-r_1} + \kappa_{hhVV}\right)(\kappa_{hVV}^2 F_1 + \kappa_{H_3^\pm hW}^2 F_2) \\ &+ \beta_h^{-1}(\kappa_{hVV}^4 F_3 + \kappa_{H_3^\pm hW}^4 F_4 + 4\kappa_{hVV}^2\kappa_{H_3^\pm hW}^2 F_5)\Bigg],\end{aligned} \tag{4.17}$$

where the functions F_i $(i = 1, \ldots, 5)$ are reproduced in appendix C and $\beta_h = (1-4r_h)^{1/2}$. Note that here r_i $(i = h,\ Z,\ H_1,\ H_3)$ are defined with respect to $\hat{s} = xs$, e.g., $r_1 = m_1^2/\hat{s}$.

The total cross section for $e^+e^- \to hh\nu_e\bar{\nu}_e$ is shown in figure 17 at $\sqrt{s} = 500$ GeV and 1 TeV respectively. It varies in a wide range as κ_{hhh} and $\kappa_{H_1^0hh}$ do, indicating its sensitivity to the values of trilinear couplings. Similarly to the case of the double Higgs-strahlung process, the cross section is strongly enhanced in the parameter range where the fusion subprocess, $WW \to H_1^0 \to hh$, is resonant also with $\kappa_{hhh} \approx 1$. Out of the resonant region the cross section decreases with increasing κ_{hhh} due to destructive interference between the scalar and gauge parts of the amplitude. From figure 13, one sees that $\kappa_{hhh} < 1$ would not be favored by HL-HLC@3000. In this case, we expect a smaller cross section in the non-resonance region.

JHEP02(2018)007

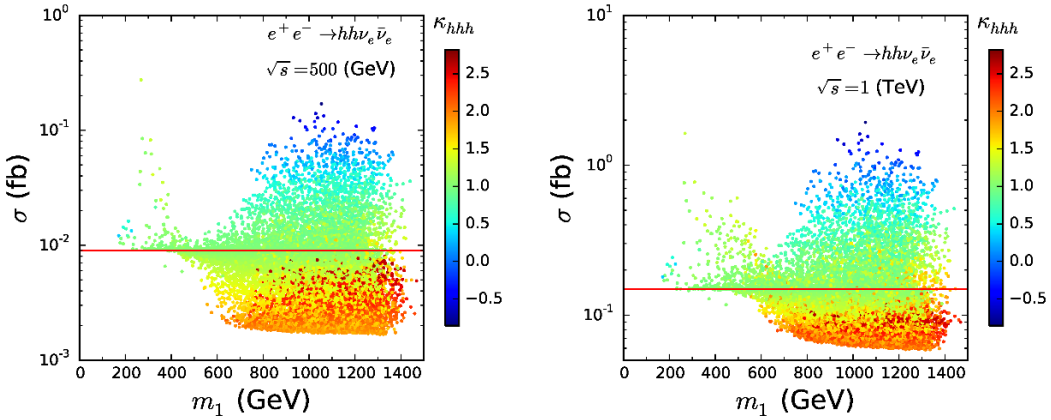

Figure 17. Cross section for $e^+e^- \to hh\nu_e\bar{\nu}_e$ as a function of the H_1^0 mass m_1 at $\sqrt{s} = 500$ GeV (left panel) and 1 TeV (right). The horizontal line indicates the SM value.

5 Conclusions

In this paper, we have investigated the dominant single and double SM-like Higgs (h) production at future e^+e^- colliders in the Georgi-Machacek (GM) model. We comprehensively considered various constraints that are currently available, including theoretical, indirect, and direct experimental constraints on the model parameters. In particular, we updated the constraints from searches for heavy singlet (H_1^0), triplet (H_3), and quintuplet (H_5) Higgs scalars and from SM-like Higgs signal strengths with the latest LHC results. The GM model parameter space now becomes more tightly constrained, for instance, only $v_\Delta \lesssim 40$ GeV with $-30^\circ \lesssim \alpha \lesssim 0^\circ$ is allowed now.

Our analysis of the Higgs production has been done in the allowed parameter regions established as above. Besides modifications to the SM couplings, the SM-like Higgs production receives new contributions from new scalars such as H_1^0, H_3^0, and can deviate significantly from the prediction in the SM. Our numerical results have the following key features:

- For single Higgs production such as $e^+e^- \to hZ$, $h\nu_e\bar{\nu}_e$, he^+e^-, the production mechanisms are the same as in SM with the only modification occurring in the Higgs-gauge boson coupling hVV. Their cross sections are modified by a factor ranging from 0.86 to 1.32.

- For associated Higgs production with a top pair $e^+e^- \to ht\bar{t}$, there is a new contribution via $e^+e^- \to hH_3^0$ with $H_3^0 \to t\bar{t}$. When $2m_t < m_3 < \sqrt{s} - m_h$ is fulfilled, H_3^0 becomes resonantly produced, thus enhancing the cross section by up to three times.

- For the double Higgs-strahlung process $e^+e^- \to hhZ$, both H_1^0 and H_3^0 contribute. When resonantly produced, they can lead to an order of magnitude enhancement in the cross section. In the non-resonant region, large deviations are still possible due to a large modification to the trilinear Higgs coupling.

JHEP02(2018)007

- For the double Higgs production via vector boson fusion $e^+e^- \to hh\nu_e\bar{\nu}_e$, both H_1^0 and $H_3^\pm$ enter but only H_1^0 can be on-shell produced. In the resonant region more than an order of magnitude enhancement is viable, and in the non-resonant region the cross section can maximally increase or decrease by an order of magnitude.

Anticipating that LHC will be operated at slightly higher energy and with larger integrated luminosity, we have also estimated its future impact on Higgs couplings and production at electron colliders. We found that LHC@300 and HL-LHC@3000 have the ability to exclude some of the parameter space that is currently allowed. When the new scalars in the GM model are light enough to be resonantly produced at electron colliders, large enhancement in the SM-like Higgs production is possible though its couplings are close to the SM values. In the non-resonance region, the double Higgs production channels are expected to deviate significantly from the SM under the strict future bounds from LHC. If the on-going LHC experiments could observe some deviations of the Higgs couplings, future electron colliders would be capable of confirming it; if not, precise measurements of the Higgs properties at future electron colliders could probe most of the currently allowed parameter space of the GM model. Compared to other popular models such as MSSM and THDM, the GM model can enhance or suppress Higgs couplings to vector bosons and fermions, and drastically change the trilinear Higgs coupling from the SM prediction. The modification of these Higgs couplings leads to distinguished phenomenology for Higgs production processes at e^+e^- colliders. Furthermore, light scalars such as H_1^0 and H_3^0 can be on-shell produced in certain processes, which provides a good chance to hunt new particles. We thus expect that the model could be tested with high precision and be discriminated from some other new physics scenarios.

Acknowledgments

This work was supported in part by the Grants No. NSFC-11575089 and No. NSFC-11025525, by The National Key Research and Development Program of China under Grant No. 2017YFA0402200, and by the CAS Center for Excellence in Particle Physics (CCEPP). We thank the anonymous referee for suggesting the inclusion of projected limits that are expected from future LHC operations.

A Coefficients for $\sigma(e^+e^- \to ht\bar{t})$

The seven coefficients G_i $(i = 1, \cdots, 7)$ appearing in eq. (4.8) can be obtained by slight adaption from the MSSM case [116, 117]. The Higgs radiation from the top quark yields the first two coefficients:

$$G_1 = \frac{2g_t^2}{s^2(\beta_t^2 - x_h^2)x_h}\Big\{ -4\beta_t(4m_t^2 - m_h^2)(2m_t^2 + s)x_h + (\beta_t^2 - x_h^2)\Big[16m_t^4 + 2m_h^4 - 2m_h^2 s x_h + s^2 x_h^2 - 4m_t^2(3m_h^2 - 2s - 2s x_h)\Big] \ln\left(\frac{x_h + \beta_t}{x_h - \beta_t}\right)\Big\}, \tag{A.1}$$

$$G_2 = \frac{-2g_t^2}{s^2(\beta_t^2 - x_h^2)x_h}\Big\{\beta_t x_h\Big[-96m_t^4 + 24m_t^2 m_h^2 - s(m_h^2 - s - s x_h)(\beta_t^2 - x_h^2)\Big] + 2(\beta_t^2 - x_h^2)\Big[24m_t^4 + 2(m_h^4 - m_h^2 s x_h) - m_t^2(14m_h^2 - 12s x_h - s x_h^2)\Big] \ln\left(\frac{x_h + \beta_t}{x_h - \beta_t}\right)\Big\}.$$

The other five coefficients all involve the Higgs radiation from the Z boson including its interference with the radiation from the top quark:

$$
\begin{aligned}
G_3 &= \frac{-2\beta_t g_Z^2 m_t^2}{m_Z^2(m_h^2-m_Z^2+s-sx_h)^2}\{4m_h^4+12m_Z^4+2m_Z^2sx_h^2+s^2(x_h-1)x_h^2 \\
&\quad -m_h^2[8m_Z^2+s(x_h^2+4x_h-4)]\}, \\
G_4 &= \frac{\beta_t g_Z^2 m_Z^2}{6(m_h^2-m_Z^2+s-sx_h)^2}[48m_t^2+12m_h^2+s(24-\beta_t^2-24x_h+3x_h^2)], \\
G_5 &= \frac{4g_t g_Z m_t}{m_Z s(m_h^2-m_Z^2+s-sx_h)}\Big\{\beta_t s\Big[6m_Z^2-x_h(m_h^2+s-sx_h)\Big] \\
&\quad +2\Big[m_h^2(m_h^2-3m_Z^2+s-sx_h)+m_t^2(12m_Z^2-4m_h^2+sx_h^2)\Big]\ln\left(\frac{x_h+\beta_t}{x_h-\beta_t}\right)\Big\}, \\
G_6 &= \frac{-8g_t g_Z m_t m_Z}{s(m_h^2-m_Z^2+s-sx_h)}\left[\beta_t s+(4m_t^2-m_h^2+2s-sx_h)\ln\left(\frac{x_h+\beta_t}{x_h-\beta_t}\right)\right], \\
G_7 &= \frac{-g_{H_3^0t\bar{t}}\kappa_{hH_3^0Z}}{m_h^2-m_{H_3}^2+s-sx_h}\Big\{2\beta_t(4m_h^2-sx_h)\left[\frac{(m_h^2+s-sx_h)g_{H_3^0t\bar{t}}\kappa_{H_3^0hZ}}{m_h^2-m_{H_3}^2+s-sx_h}-\frac{2m_t g_Z}{m_Z}\right] \\
&\quad +\frac{2g_t}{s}[2sx_h\beta_t(sx_h-s-m_h^2)-4(m_h^2(sx_h-s-m_h^2)+m_t^2(4m_h^2-sx_h^2))]\ln\left(\frac{x_h+\beta_t}{x_h-\beta_t}\right)\Big\}.
\end{aligned}
\tag{A.2}
$$

The relevant h couplings are defined in terms of their κ factors:

$$
g_Z=\frac{m_Z}{v}\kappa_{hVV},\ g_t=-\frac{m_t}{v}\kappa_{ht\bar{t}},\ g_{H_3^0t\bar{t}}=\frac{m_t}{v}\kappa_{H_3^0t\bar{t}}. \tag{A.3}
$$

The kinematical variable β_t is

$$
\beta_t=\left\{\frac{[x_h^2-(x_h^{\min})^2](x_h^{\max}-x_h)}{x_h^{\max}-x_h+4r_t}\right\}^{1/2}, \tag{A.4}
$$

where $x_h^{\min}=2r_h^{1/2}$ and $x_h^{\max}=1-4r_t+r_h$.

B Trilinear Higgs couplings

The trilinear Higgs couplings used in our calculation include

$$
\begin{aligned}
g_{hhh} &= 24\lambda_1 c_\alpha^3 v_\phi+\frac{3\sqrt{3}}{2}c_\alpha^2 s_\alpha\left[M_1+4\left(\lambda_5-2\lambda_2\right)v_\Delta\right]+6\left(2\lambda_2-\lambda_5\right)c_\alpha s_\alpha^2 v_\phi \\
&\quad +4\sqrt{3}s_\alpha^3\left[M_2-2\left(\lambda_3+3\lambda_4\right)v_\Delta\right], \\
g_{H_1^0hh} &= 4\left(6\lambda_1-2\lambda_2+\lambda_5\right)c_\alpha^2 s_\alpha v_\phi+2\left(2\lambda_2-\lambda_5\right)s_\alpha^3 v_\phi \\
&\quad +\sqrt{3}c_\alpha s_\alpha^2\left[M_1-4M_2+4\left(2\lambda_3-2\lambda_2+6\lambda_4+\lambda_5\right)v_\Delta\right] \\
&\quad -\frac{\sqrt{3}}{2}c_\alpha^3\left[M_1+4\left(\lambda_5-2\lambda_2\right)v_\Delta\right].
\end{aligned}
\tag{B.1}
$$

In the decoupling limit, $s_\alpha, v_\Delta, M_1, M_2 \to 0$, and $\lambda_1 \to m_h^2/(8v^2)$, we have $g_{hhh} \to 24v\lambda_1 \to 3m_h^2/v$ and $g_{H_1^0hh} \to -\sqrt{3}M_1/2 \to 0$.

JHEP02(2018)007

C Coefficients for $\sigma(e^+e^- \to hh\nu_e\bar{\nu}_e)$

The coefficients used in the calculation of $e^+e^- \to hh\nu_e\bar{\nu}_e$ are [119]

$$
\begin{aligned}
F_1 &= 8[2r_W + (r_h - r_W)^2]l_W - 4\beta_h(1 + 2r_h - 2r_W),\\
F_2 &= 8(r_h - r_3)^2 l_3 - 4\beta_h(1 + 2r_h - 2r_w),\\
F_3 &= 8\beta_h[2r_W + (r_h - r_W)^2][2r_W + 1 - 3(r_h - r_W)^2]\frac{l_W}{a_W}\\
&\quad + 16[2r_W + (r_h - r_W)^2]^2 y_W + 16\beta_h^2(1 + a_W)^2,\\
F_4 &= 8\beta_h(r_h - r_3)^2[1 - 3(r_h - r_3)^2]\frac{l_3}{a_3}\\
&\quad + 16(r_h - r_3)^4 y_3 + 16\beta_h^2(1 + a_3)^2,\\
F_5 &= \frac{\beta_h}{4}(z_W l_W + z_3 l_3) + 8\beta_h^2(1 + a_W)(1 + a_3),
\end{aligned}
\tag{C.1}
$$

where

$$
\begin{aligned}
l_{W,3} &= \ln\frac{1 - 2r_h + 2r_{W,3} - \beta_h}{1 - 2r_h + 2r_{W,3} + \beta_h},\\
y_{W,3} &= \frac{2\beta_h^2}{(1 - 2r_h + 2r_{W,3})^2 - \beta_h^2},\\
a_{W,3} &= -\frac{1}{2} + r_h - r_{W,3},\\
z_W &= \frac{(1 + 2a_W)^2}{a_3 - a_W}[8r_W + (1 + 2a_W)^2] + \frac{(1 - 2a_W)^2}{a_3 + a_W}[8r_W + (1 + 2a_W)^2],\\
z_3 &= -\frac{(1 + 2a_3)^2}{a_3 - a_W}[8r_W + (1 + 2a_3)^2] + \frac{(1 + 2a_3)^2}{a_3 + a_W}[8r_W + (1 - 2a_3)^2].
\end{aligned}
\tag{C.2}
$$

References

[1] ATLAS collaboration, *Observation of a new particle in the search for the standard model Higgs boson with the ATLAS detector at the LHC*, *Phys. Lett.* **B 716** (2012) 1 [arXiv:1207.7214] [INSPIRE].

[2] CMS collaboration, *Observation of a new boson at a mass of* 125 *GeV with the CMS experiment at the LHC*, *Phys. Lett.* **B 716** (2012) 30 [arXiv:1207.7235] [INSPIRE].

[3] F. Englert and R. Brout, *Broken symmetry and the mass of gauge vector mesons*, *Phys. Rev. Lett.* **13** (1964) 321 [INSPIRE].

[4] P.W. Higgs, *Broken symmetries, massless particles and gauge fields*, *Phys. Lett.* **12** (1964) 132 [INSPIRE].

[5] P.W. Higgs, *Broken symmetries and the masses of gauge bosons*, *Phys. Rev. Lett.* **13** (1964) 508 [INSPIRE].

JHEP02(2018)007

[6] G.S. Guralnik, C.R. Hagen and T.W.B. Kibble, *Global conservation laws and massless particles*, *Phys. Rev. Lett.* **13** (1964) 585 [INSPIRE].

[7] P.W. Higgs, *Spontaneous symmetry breakdown without massless bosons*, *Phys. Rev.* **145** (1966) 1156 [INSPIRE].

[8] T.W.B. Kibble, *Symmetry breaking in nonAbelian gauge theories*, *Phys. Rev.* **155** (1967) 1554 [INSPIRE].

[9] H.P. Nilles, *Supersymmetry, supergravity and particle physics*, *Phys. Rept.* **110** (1984) 1 [INSPIRE].

[10] H.E. Haber and G.L. Kane, *The search for supersymmetry: probing physics beyond the standard model*, *Phys. Rept.* **117** (1985) 75 [INSPIRE].

[11] A. Djouadi, *The anatomy of electro-weak symmetry breaking. II. The Higgs bosons in the minimal supersymmetric model*, *Phys. Rept.* **459** (2008) 1 [hep-ph/0503173] [INSPIRE].

[12] J.-J. Cao, Z.-X. Heng, J.M. Yang, Y.-M. Zhang and J.-Y. Zhu, *A SM-like Higgs near 125 GeV in low energy SUSY: a comparative study for MSSM and NMSSM*, *JHEP* **03** (2012) 086 [arXiv:1202.5821] [INSPIRE].

[13] E. Ma, *Naturally small seesaw neutrino mass with no new physics beyond the TeV scale*, *Phys. Rev. Lett.* **86** (2001) 2502 [hep-ph/0011121] [INSPIRE].

[14] S.M. Davidson and H.E. Logan, *Dirac neutrinos from a second Higgs doublet*, *Phys. Rev.* **D 80** (2009) 095008 [arXiv:0906.3335] [INSPIRE].

[15] N. Haba and K. Tsumura, *ν-two Higgs doublet model and its collider phenomenology*, *JHEP* **06** (2011) 068 [arXiv:1105.1409] [INSPIRE].

[16] G.C. Branco et al., *Theory and phenomenology of two-Higgs-doublet models*, *Phys. Rept.* **516** (2012) 1 [arXiv:1106.0034] [INSPIRE].

[17] W. Wang and Z.-L. Han, *Global $\mathrm{U}(1)_L$ breaking in neutrinophilic 2HDM: from lhc signatures to X-ray line*, *Phys. Rev.* **D 94** (2016) 053015 [arXiv:1605.00239] [INSPIRE].

[18] C. Guo, S.-Y. Guo, Z.-L. Han, B. Li and Y. Liao, *Hunting for heavy Majorana neutrinos with lepton number violating signatures at LHC*, *JHEP* **04** (2017) 065 [arXiv:1701.02463] [INSPIRE].

[19] N. Arkani-Hamed, A.G. Cohen and H. Georgi, *Electroweak symmetry breaking from dimensional deconstruction*, *Phys. Lett.* **B 513** (2001) 232 [hep-ph/0105239] [INSPIRE].

[20] N. Arkani-Hamed, A.G. Cohen, T. Gregoire and J.G. Wacker, *Phenomenology of electroweak symmetry breaking from theory space*, *JHEP* **08** (2002) 020 [hep-ph/0202089] [INSPIRE].

[21] N. Arkani-Hamed et al., *The minimal moose for a little Higgs*, *JHEP* **08** (2002) 021 [hep-ph/0206020] [INSPIRE].

[22] I. Low, W. Skiba and D. Tucker-Smith, *Little Higgses from an antisymmetric condensate*, *Phys. Rev.* **D 66** (2002) 072001 [hep-ph/0207243] [INSPIRE].

[23] T. Han, H.E. Logan, B. McElrath and L.-T. Wang, *Phenomenology of the little Higgs model*, *Phys. Rev.* **D 67** (2003) 095004 [hep-ph/0301040] [INSPIRE].

[24] K. Agashe, R. Contino and A. Pomarol, *The minimal composite Higgs model*, *Nucl. Phys.* **B 719** (2005) 165 [hep-ph/0412089] [INSPIRE].

[25] B. Gripaios, A. Pomarol, F. Riva and J. Serra, *Beyond the minimal composite Higgs model*, *JHEP* **04** (2009) 070 [arXiv:0902.1483] [INSPIRE].

[26] D. Marzocca, M. Serone and J. Shu, *General composite Higgs models*, *JHEP* **08** (2012) 013 [arXiv:1205.0770] [INSPIRE].

JHEP02(2018)007

[27] M. Dührssen et al., *Extracting Higgs boson couplings from CERN LHC data*, *Phys. Rev.* **D 70** (2004) 113009 [hep-ph/0406323] [INSPIRE].

[28] R. Lafaye, T. Plehn, M. Rauch and D. Zerwas, *Higgs factories: Higgsstrahlung versus W fusion*, *Phys. Rev.* **D 96** (2017) 075044 [arXiv:1706.02174] [INSPIRE].

[29] CEPC-SPPC study group, *CEPC-SPPC preliminary conceptual design report. 1. Physics and Detector* IHEP-CEPC-DR-2015-01 (2015) [IHEP-TH-2015-01] [IHEP-EP-2015-01].

[30] CEPC-SPPC study group, *CEPC-SPPC preliminary conceptual design report. 2. Accelerator*, IHEP-CEPC-DR-2015-01 (2015) [IHEP-AC-2015-01].

[31] TLEP Design Study Working Group collaboration, M. Bicer et al., *First look at the physics case of TLEP*, *JHEP* **01** (2014) 164 [arXiv:1308.6176] [INSPIRE].

[32] M. Aicheler et al., *A multi-TeV linear collider based on CLIC technology: CLIC conceptual design report*, CERN-2012-007 (2012).

[33] H. Abramowicz et al., *Higgs physics at the CLIC electron-positron linear collider*, *Eur. Phys. J.* **C 77** (2017) 475 [arXiv:1608.07538] [INSPIRE].

[34] H. Baer et al., *The International Linear Collider technical design report — Volume 2: physics*, arXiv:1306.6352 [INSPIRE].

[35] D.M. Asner et al., *ILC Higgs white paper*, arXiv:1310.0763 [INSPIRE].

[36] K. Fujii et al., *Physics case for the International Linear Collider*, arXiv:1506.05992 [INSPIRE].

[37] C.-x. Yue, S.-z. Wang and D.-q. Yu, *Littlest Higgs model and associated ZH production at high energy e^+e^- collider*, *Phys. Rev.* **D 68** (2003) 115004 [hep-ph/0309113] [INSPIRE].

[38] C.-X. Yue, W. Wang, Z.-J. Zong and F. Zhang, *Probing signals of the littlest Higgs model via the WW fusion processes at the high energy e^+e^- collider*, *Eur. Phys. J.* **C 42** (2005) 331 [hep-ph/0504253] [INSPIRE].

[39] Y.-B. Liu, L.-L. Du and X.-L. Wang, *Higgs boson pair production process $e^+e^- \to ZHH$ in the littlest Higgs model at the ILC*, *J. Phys.* **G 33** (2007) 577 [hep-ph/0609208] [INSPIRE].

[40] A. Arhrib, R. Benbrik and C.-W. Chiang, *Probing triple Higgs couplings of the two Higgs doublet model at linear collider*, *Phys. Rev.* **D 77** (2008) 115013 [arXiv:0802.0319] [INSPIRE].

[41] D. Lopez-Val and J. Solà, *Neutral Higgs-pair production at linear colliders within the general 2HDM: quantum effects and triple Higgs boson self-interactions*, *Phys. Rev.* **D 81** (2010) 033003 [arXiv:0908.2898] [INSPIRE].

[42] E. Asakawa, D. Harada, S. Kanemura, Y. Okada and K. Tsumura, *Higgs boson pair production in new physics models at hadron, lepton and photon colliders*, *Phys. Rev.* **D 82** (2010) 115002 [arXiv:1009.4670] [INSPIRE].

[43] Z. Heng, L. Shang and P. Wan, *Pair production of a 125 GeV Higgs boson in MSSM and NMSSM at the ILC*, *JHEP* **10** (2013) 047 [arXiv:1306.0279] [INSPIRE].

[44] B. Yang, J. Han, S. Zhou and N. Liu, *Single Higgs boson production at e^+e^- colliders in the Littlest Higgs Model with T-parity*, *J. Phys.* **G 41** (2014) 075009 [arXiv:1401.0289] [INSPIRE].

[45] B. Yang, Z. Liu, N. Liu and J. Han, *Double Higgs production in the littlest Higgs model with T-parity at high energy e^+e^- colliders*, *Eur. Phys. J.* **C 74** (2014) 3203 [arXiv:1408.4295] [INSPIRE].

JHEP02(2018)007

[46] Y.-B. Liu and Z.-J. Xiao, *Single Higgs boson production at the ILC in the left-right twin Higgs model*, *J. Phys.* **G 42** (2015) 065005 [arXiv:1412.5905] [INSPIRE].

[47] J. Han, S. Li, B. Yang and N. Liu, *Higgs boson production and decay at e^+e^- colliders as a probe of the left-right twin Higgs model*, *Nucl. Phys.* **B 896** (2015) 200 [arXiv:1504.08236] [INSPIRE].

[48] S. Antusch, E. Cazzato and O. Fischer, *Higgs production from sterile neutrinos at future lepton colliders*, *JHEP* **04** (2016) 189 [arXiv:1512.06035] [INSPIRE].

[49] S. Kanemura, K. Kaneta, N. Machida, S. Odori and T. Shindou, *Single and double production of the Higgs boson at hadron and lepton colliders in minimal composite Higgs models*, *Phys. Rev.* **D 94** (2016) 015028 [arXiv:1603.05588] [INSPIRE].

[50] C.K. Khosa and P.N. Pandita, *Measuring the trilinear neutral Higgs boson couplings in the minimal supersymmetric standard model at e^+e^- colliders in the light of the discovery of a Higgs boson*, *Int. J. Mod. Phys.* **A 31** (2016) 1650108 [arXiv:1606.02093] [INSPIRE].

[51] S. De Curtis, S. Moretti, K. Yagyu and E. Yildirim, *Single and double SM-like Higgs boson production at future electron-positron colliders in composite 2HDMs*, *Phys. Rev.* **D 95** (2017) 095026 [arXiv:1702.07260] [INSPIRE].

[52] Y.-C. Guo, C.-X. Yue and Z.-C. Liu, *Double elementary Goldstone Higgs boson production in future linear colliders*, arXiv:1709.00648 [INSPIRE].

[53] J. Gu, H. Li, Z. Liu, S. Su and W. Su, *Learning from Higgs physics at future Higgs factories*, *JHEP* **12** (2017) 153 [arXiv:1709.06103] [INSPIRE].

[54] H. Georgi and M. Machacek, *Doubly charged Higgs bosons*, *Nucl. Phys.* **B 262** (1985) 463 [INSPIRE].

[55] M.S. Chanowitz and M. Golden, *Higgs boson triplets with $M(W) = M(Z)\cos\theta\omega$*, *Phys. Lett.* **B 165** (1985) 105.

[56] S. Chang and J.G. Wacker, *Little Higgs and custodial* SU(2), *Phys. Rev.* **D 69** (2004) 035002 [hep-ph/0303001] [INSPIRE].

[57] S. Chang, *A 'Littlest Higgs' model with custodial* SU(2) *symmetry*, *JHEP* **12** (2003) 057 [hep-ph/0306034] [INSPIRE].

[58] L. Cort, M. Garcia and M. Quirós, *Supersymmetric custodial triplets*, *Phys. Rev.* **D 88** (2013) 075010 [arXiv:1308.4025] [INSPIRE].

[59] R. Vega, R. Vega-Morales and K. Xie, *The supersymmetric Georgi-Machacek model*, arXiv:1711.05329 [INSPIRE].

[60] H.E. Logan and V. Rentala, *All the generalized Georgi-Machacek models*, *Phys. Rev.* **D 92** (2015) 075011 [arXiv:1502.01275] [INSPIRE].

[61] R. Campbell, S. Godfrey, H.E. Logan and A. Poulin, *Real singlet scalar dark matter extension of the Georgi-Machacek model*, *Phys. Rev.* **D 95** (2017) 016005 [arXiv:1610.08097] [INSPIRE].

[62] T. Pilkington, *Dark matter in the Georgi-Machacek model with an additional inert doublet*, arXiv:1711.04378 [INSPIRE].

[63] H.E. Haber and H.E. Logan, *Radiative corrections to the $Zb\bar{b}$ vertex and constraints on extended Higgs sectors*, *Phys. Rev.* **D 62** (2000) 015011 [hep-ph/9909335] [INSPIRE].

[64] S. Godfrey and K. Moats, *Exploring Higgs triplet models via vector boson scattering at the LHC*, *Phys. Rev.* **D 81** (2010) 075026 [arXiv:1003.3033] [INSPIRE].

JHEP02(2018)007

[65] H.E. Logan and M.-A. Roy, *Higgs couplings in a model with triplets*, *Phys. Rev.* **D 82** (2010) 115011 [arXiv:1008.4869] [INSPIRE].

[66] S. Chang, C.A. Newby, N. Raj and C. Wanotayaroj, *Revisiting theories with enhanced Higgs couplings to weak gauge bosons*, *Phys. Rev.* **D 86** (2012) 095015 [arXiv:1207.0493] [INSPIRE].

[67] C.-W. Chiang and K. Yagyu, *Testing the custodial symmetry in the Higgs sector of the Georgi-Machacek model*, *JHEP* **01** (2013) 026 [arXiv:1211.2658] [INSPIRE].

[68] S. Kanemura, M. Kikuchi and K. Yagyu, *Probing exotic Higgs sectors from the precise measurement of Higgs boson couplings*, *Phys. Rev.* **D 88** (2013) 015020 [arXiv:1301.7303] [INSPIRE].

[69] C. Englert, E. Re and M. Spannowsky, *Triplet Higgs boson collider phenomenology after the LHC*, *Phys. Rev.* **D 87** (2013) 095014 [arXiv:1302.6505] [INSPIRE].

[70] C. Englert, E. Re and M. Spannowsky, *Pinning down Higgs triplets at the LHC*, *Phys. Rev.* **D 88** (2013) 035024 [arXiv:1306.6228] [INSPIRE].

[71] C.-W. Chiang, A.-L. Kuo and K. Yagyu, *Enhancements of weak gauge boson scattering processes at the CERN LHC*, *JHEP* **10** (2013) 072 [arXiv:1307.7526] [INSPIRE].

[72] A. Efrati and Y. Nir, *What if* $\lambda_{hhh} \neq 3m_h^2/v$, arXiv:1401.0935 [INSPIRE].

[73] C.-W. Chiang and T. Yamada, *Electroweak phase transition in Georgi-Machacek model*, *Phys. Lett.* **B 735** (2014) 295 [arXiv:1404.5182] [INSPIRE].

[74] S.I. Godunov, M.I. Vysotsky and E.V. Zhemchugov, *Suppression of* $H \to VV$ *decay channels in the Georgi-Machacek model*, *Phys. Lett.* **B 751** (2015) 505 [arXiv:1505.05039] [INSPIRE].

[75] C.-W. Chiang, S. Kanemura and K. Yagyu, *Phenomenology of the Georgi-Machacek model at future electron-positron colliders*, *Phys. Rev.* **D 93** (2016) 055002 [arXiv:1510.06297] [INSPIRE].

[76] C.-W. Chiang, A.-L. Kuo and T. Yamada, *Searches of exotic Higgs bosons in general mass spectra of the Georgi-Machacek model at the LHC*, *JHEP* **01** (2016) 120 [arXiv:1511.00865] [INSPIRE].

[77] C. Degrande et al., *Automatic predictions in the Georgi-Machacek model at next-to-leading order accuracy*, *Phys. Rev.* **D 93** (2016) 035004 [arXiv:1512.01243] [INSPIRE].

[78] M.A. Arroyo-Urena, G. Hernandez-Tome and G. Tavares-Velasco, WWV $(V = \gamma, Z)$ *vertex in the Georgi-Machacek model*, *Phys. Rev.* **D 94** (2016) 095006 [arXiv:1610.04911] [INSPIRE].

[79] S. Blasi, S. De Curtis and K. Yagyu, *Effects of custodial symmetry breaking in the Georgi-Machacek model at high energies*, *Phys. Rev.* **D 96** (2017) 015001 [arXiv:1704.08512] [INSPIRE].

[80] Y. Zhang, H. Sun, X. Luo and W. Zhang, *Searching for the heavy charged custodial fiveplet Higgs boson in the Georgi-Machacek model at the International Linear Collider*, *Phys. Rev.* **D 95** (2017) 115022 [arXiv:1706.01490] [INSPIRE].

[81] C.-W. Chiang, A.-L. Kuo and K. Yagyu, *Radiative corrections to Higgs couplings with weak gauge bosons in custodial multi-Higgs models*, *Phys. Lett.* **B 774** (2017) 119 [arXiv:1707.04176] [INSPIRE].

[82] C. Degrande, K. Hartling and H.E. Logan, *Scalar decays to* $\gamma\gamma$, $Z\gamma$ *and* $W\gamma$ *in the Georgi-Machacek model*, *Phys. Rev.* **D 96** (2017) 075013 [arXiv:1708.08753] [INSPIRE].

JHEP02(2018)007

[83] H.E. Logan and M.B. Reimer, *Characterizing a benchmark scenario for heavy Higgs boson searches in the Georgi-Machacek model*, *Phys. Rev.* **D 96** (2017) 095029 [arXiv:1709.01883] [INSPIRE].

[84] M.E. Krauss and F. Staub, *Perturbativity constraints in BSM models*, arXiv:1709.03501 [INSPIRE].

[85] H. Sun, X. Luo, W. Wei and T. Liu, *Searching for the doubly-charged Higgs bosons in the Georgi-Machacek model at the electron-proton colliders*, *Phys. Rev.* **D 96** (2017) 095003 [arXiv:1710.06284] [INSPIRE].

[86] K. Hartling, K. Kumar and H.E. Logan, *The decoupling limit in the Georgi-Machacek model*, *Phys. Rev.* **D 90** (2014) 015007 [arXiv:1404.2640] [INSPIRE].

[87] M. Aoki and S. Kanemura, *Unitarity bounds in the Higgs model including triplet fields with custodial symmetry*, *Phys. Rev.* **D 77** (2008) 095009 [arXiv:0712.4053] [INSPIRE].

[88] J.F. Gunion, R. Vega and J. Wudka, *Naturalness problems for $\rho = 1$ and other large one loop effects for a standard model Higgs sector containing triplet fields*, *Phys. Rev.* **D 43** (1991) 2322 [INSPIRE].

[89] ATLAS and CMS collaboration, *Combined measurement of the Higgs boson mass in pp collisions at $\sqrt{s} = 7$ and 8 TeV with the ATLAS and CMS experiments*, *Phys. Rev. Lett.* **114** (2015) 191803 [arXiv:1503.07589] [INSPIRE].

[90] K. Hartling, K. Kumar and H.E. Logan, *Indirect constraints on the Georgi-Machacek model and implications for Higgs boson couplings*, *Phys. Rev.* **D 91** (2015) 015013 [arXiv:1410.5538] [INSPIRE].

[91] K. Hartling, K. Kumar and H.E. Logan, *GMCALC: a calculator for the Georgi-Machacek model*, arXiv:1412.7387 [INSPIRE].

[92] ATLAS collaboration, *Projections for measurements of Higgs boson signal strengths and coupling parameters with the ATLAS detector at a HL-LHC*, ATL-PHYS-PUB-2014-016 (2014).

[93] ATLAS collaboration, *Search for a high-mass Higgs boson decaying to a pair of W bosons in pp collisions at $\sqrt{s} = 13$ TeV with the ATLAS detector*, ATLAS-CONF-2016-074 (2016).

[94] ATLAS collaboration, *Searches for heavy ZZ and ZW resonances in the llqq and vvqq final states in pp collisions at $\sqrt{s} = 13$ TeV with the ATLAS detector*, ATLAS-CONF-2016-082 (2016).

[95] LHC Higgs Cross Section Working Group collaboration, J.R. Andersen et al., *Handbook of LHC Higgs cross sections: 3. Higgs properties*, arXiv:1307.1347 [INSPIRE].

[96] J. Chang, C.-R. Chen and C.-W. Chiang, *Higgs boson pair productions in the Georgi-Machacek model at the LHC*, *JHEP* **03** (2017) 137 [arXiv:1701.06291] [INSPIRE].

[97] CMS collaboration, *Search for resonant and nonresonant Higgs boson pair production in the $b\bar{b}\ell\nu\ell\nu$ final state in proton-proton collisions at $\sqrt{s} = 13$ TeV*, *JHEP* **01** (2018) 054 [arXiv:1708.04188] [INSPIRE].

[98] C.-W. Chiang and K. Tsumura, *Properties and searches of the exotic neutral Higgs bosons in the Georgi-Machacek model*, *JHEP* **04** (2015) 113 [arXiv:1501.04257] [INSPIRE].

[99] ATLAS collaboration, *Search for a CP-odd Higgs boson decaying to Zh in pp collisions at $\sqrt{s} = 8$ TeV with the ATLAS detector*, *Phys. Lett.* **B 744** (2015) 163 [arXiv:1502.04478] [INSPIRE].

[100] ATLAS collaboration, *Search for a CP-odd Higgs boson decaying to Zh in pp collisions at $\sqrt{s} = 13$ TeV with the ATLAS detector*, ATLAS-CONF-2016-015 (2016).

JHEP02(2018)007

[101] ATLAS collaboration, *Search for heavy Higgs bosons A/H decaying to a top quark pair in pp collisions at $\sqrt{s} = 8$ TeV with the ATLAS detector*, *Phys. Rev. Lett.* **119** (2017) 191803 [arXiv:1707.06025] [INSPIRE].

[102] ATLAS collaboration, *Search for charged Higgs bosons decaying via $H^{\pm} \to \tau^{\pm}\nu$ in fully hadronic final states using pp collision data at $\sqrt{s} = 8$ TeV with the ATLAS detector*, *JHEP* **03** (2015) 088 [arXiv:1412.6663] [INSPIRE].

[103] CMS collaboration, *Search for a charged Higgs boson in pp collisions at $\sqrt{s} = 8$ TeV*, *JHEP* **11** (2015) 018 [arXiv:1508.07774] [INSPIRE].

[104] ATLAS collaboration, *Search for a charged Higgs boson produced in the vector-boson fusion mode with decay $H^{\pm} \to W^{\pm}Z$ using pp collisions at $\sqrt{s} = 8$ TeV with the ATLAS experiment*, *Phys. Rev. Lett.* **114** (2015) 231801 [arXiv:1503.04233] [INSPIRE].

[105] CMS collaboration, *Search for charged Higgs bosons in WZ decays at 13 TeV*, CMS-PAS-HIG-16-027 (2016).

[106] C.-W. Chiang, S. Kanemura and K. Yagyu, *Novel constraint on the parameter space of the Georgi-Machacek model with current LHC data*, *Phys. Rev.* **D 90** (2014) 115025 [arXiv:1407.5053] [INSPIRE].

[107] CMS collaboration, *Observation of electroweak production of same-sign W boson pairs in the two jet and two same-sign lepton final state in proton-proton collisions at $\sqrt{s} = 13$ TeV*, arXiv:1709.05822 [INSPIRE].

[108] S. Kanemura, M. Kikuchi, H. Yokoya and K. Yagyu, *LHC Run-I constraint on the mass of doubly charged Higgs bosons in the same-sign diboson decay scenario*, *PTEP* **2015** (2015) 051B02 [arXiv:1412.7603] [INSPIRE].

[109] OPAL collaboration, G. Abbiendi et al., *Decay mode independent searches for new scalar bosons with the OPAL detector at LEP*, *Eur. Phys. J.* **C 27** (2003) 311 [hep-ex/0206022] [INSPIRE].

[110] V.D. Barger, J.L. Hewett and R.J.N. Phillips, *New constraints on the charged Higgs sector in two Higgs doublet models*, *Phys. Rev.* **D 41** (1990) 3421 [INSPIRE].

[111] G. Bélanger et al., *Global fit to Higgs signal strengths and couplings and implications for extended Higgs sectors*, *Phys. Rev.* **D 88** (2013) 075008 [arXiv:1306.2941] [INSPIRE].

[112] ATLAS and CMS collaboration, *Measurements of the Higgs boson production and decay rates and constraints on its couplings from a combined ATLAS and CMS analysis of the LHC pp collision data at $\sqrt{s} = 7$ and 8 TeV*, *JHEP* **08** (2016) 045 [arXiv:1606.02266] [INSPIRE].

[113] V.D. Barger, K.-m. Cheung, A. Djouadi, B.A. Kniehl and P.M. Zerwas, *Higgs bosons: intermediate mass range at e^+e^- colliders*, *Phys. Rev.* **D 49** (1994) 79 [hep-ph/9306270] [INSPIRE].

[114] A. Djouadi et al., *Higgs particles*, in the proceedings of *e^+e^- collisions at TeV energies: the physics potential*, Annecy/Gran Sasso/Hamburg (1995), hep-ph/9605437 [INSPIRE].

[115] K.J.F. Gaemers and G.J. Gounaris, *Bremsstrahlung production of Higgs bosons in e^+e^- collisions*, *Phys. Lett.* **B 77** (1978) 379.

[116] A. Djouadi, J. Kalinowski and P.M. Zerwas, *Measuring the $Ht\bar{t}$ coupling in e^+e^- collisions*, *Mod. Phys. Lett.* **A 7** (1992) 1765 [INSPIRE].

[117] A. Djouadi, J. Kalinowski and P.M. Zerwas, *Higgs radiation off top quarks in high-energy e^+e^- colliders*, *Z. Phys.* **C 54** (1992) 255 [INSPIRE].

JHEP02(2018)007

[118] A. Djouadi, H.E. Haber and P.M. Zerwas, *Multiple production of MSSM neutral Higgs bosons at high-energy e^+e^- colliders*, *Phys. Lett.* **B 375** (1996) 203 [hep-ph/9602234] [INSPIRE].

[119] P. Osland and P.N. Pandita, *Measuring the trilinear couplings of MSSM neutral Higgs bosons at high-energy e^+e^- colliders*, *Phys. Rev.* **D 59** (1999) 055013 [hep-ph/9806351] [INSPIRE].

[120] A. Djouadi, W. Kilian, M. Muhlleitner and P.M. Zerwas, *Testing Higgs selfcouplings at e^+e^- linear colliders*, *Eur. Phys. J.* **C 10** (1999) 27 [hep-ph/9903229] [INSPIRE].

JHEP02(2018)007